Vehicular Communication in Obstructed and Non Line-of-Sight Scenarios

Vlastaras, Dimitrios

2017

Document Version:
Publisher's PDF, also known as Version of record

Vehicular Communication in Obstructed and Non Line-of-Sight Scenarios

—

Dimitrios Vlastaras

Lund 2017

Licentiate Thesis

Department of Electrical and Information Technology
Lund University
Box 118, SE-221 00 LUND
SWEDEN

This thesis is set in Computer Modern 10pt
with the LaTeX Documentation System

Series of licentiate and doctoral theses
No. 97
ISSN 1654-790X
ISBN 978-91-7753-161-6 (print)
ISBN 978-91-7753-162-3 (pdf)

Contact: dimitrios@vlastaras.se

Printed in Sweden by *Tryckeriet i E-huset*, Lund.
January 2017.

"Ἓν οἶδα ὅτι οὐδὲν οἶδα."

— Socrates

Abstract

Since the invention of the first car available to masses, the 1908 Ford Model T, technology has advanced towards making car travel safer for occupants and bystanders. In recent years, wireless communication has been introduced in the vehicular industry as a means to avoid accidents and save lives.

Wireless communication may sometimes be challenging due to obstacles in the physical world that interact with wireless signals. Such obstacles may be dynamic, e.g. other vehicles in the traffic flow, or static, e.g. nearby buildings. Two scenarios are defined to describe those cases. The obstructed line-of-sight (OLOS) scenario is described as the case where a smaller obstacle, usually a vehicle, is placed in-between a transmitter and a receiver. This obstacle usually partially blocks communication and the receiver often moves in an out of the line-of-sight. The non line-of-sight (NLOS) scenario is described as the case where a larger obstacle completely blocks communication between a transmitter and a receiver. An example would be a building at an intersection which shadows the communication between two vehicles. In this thesis the OLOS and NLOS scenarios are investigated from different points of view.

In chapter 2, a road side unit (RSU) that has been constructed and evaluated for integrating older vehicles without wireless communication with newer vehicles using wireless communication is described. Older vehicles are being detected using a universal medium-range radar and their position and velocity vectors are broadcasted wirelessly to newer vehicles. Tests have been performed by using the system in parallel with wireless enabled vehicles; by comparing the content in the messages obtained from both systems, the RSU has been found to perform adequately. Accuracy tests have been performed on the system and Kalman filtering has been applied to improve the accuracy even further.

Chapter 3 focuses on the OLOS scenario. A truck as an obstacle for wireless vehicular communication is being investigated. Real life measurements have been performed to characterize and model the wireless channel around the truck. The distance dependent path loss and additional shadowing loss due to the truck is analyzed through dynamic measurements. The large-scale

fading, delay and Doppler spreads are characterized as a measure of the channel dispersion in the time and frequency domains. It has been found that a truck as an obstacle reduces the received power by 12 and 13 dB on average in rural and highway scenarios, respectively. Also, the dispersion in time and frequency domains is highly increased when the line-of-sight is obstructed by the truck. A model for power contributions due to diffraction around the truck has also been proposed and evaluated using the previously mentioned real life measurements. It has been found that communication may actually be possible using solely diffraction around a truck as a propagation mechanism.

Finally, in chapter 4 a wireless channel emulator that has been constructed and evaluated is described. Modem manufacturers face a challenge when designing and implementing equipment for highly dynamic environments found in vehicular communication. For testing and evaluation real-life measurements with vehicles are required, which is often an expensive and slow process. The channel emulator proposed is designed and implemented using a software defined radio (SDR). The emulator together with the proposed test methodology enables quick on-bench evaluation of wireless modems. It may also be used to evaluate modem performance in different NLOS and OLOS scenarios.

Preface

This licentiate thesis concludes my work as a doctoral student. It gives an overview of the research field in which I have been working during my doctoral studies and describes my contributions to it. The scientific work in this thesis is based on the following publications, in chronological order:

[1] D. Vlastaras & F. Tufvesson, "A model for power contributions from diffraction around a truck in Vehicle-to-Vehicle communications" in *Proc. of 15th International Conference on ITS Telecommunications (ITST)*, IEEE, Warsaw, Poland, May 2017. [Submitted]

[2] D. Vlastaras, S. Malkowsky & F. Tufvesson, "Stress Test Of Vehicular Communication Transceivers Using Software Defined Radio" in *Proc. of 81st Vehicular Technology Conference (VTC)*, IEEE, Glasgow, Scotland, p. 1–4, May 2015.

[3] D. Vlastaras, T. Abbas, M. Nilsson, R. Whiton, M. Olbäck & F. Tufvesson, "Impact of a Truck as an Obstacle on Vehicle-to-Vehicle Communications in Rural and Highway Scenarios" in *Proc. of 6th International Symposium on Wireless Vehicular Communications (WiVeC)*, IEEE, Vancouver, Canada, p. 1–6, September 2014.

[4] D. Vlastaras, T. Abbas, D. Leston & F. Tufvesson, "Vehicle Detection through Wireless Vehicular Communication" in *EURASIP Journal on Wireless Communications and Networking*, p. 146–153, September 2014.

[5] D. Vlastaras, T. Abbas, D. Leston & F. Tufvesson, "Universal Medium Range Radar and IEEE 802.11p Modem Solution for Integrated Traffic Safety" in *Proc. of 13th International Conference on ITS Telecommunications (ITST)*, IEEE, p. 193–197, 2013.

During my doctoral studies, I have also contributed to the following publications. However, these publications are not included in this thesis:

[6] G. Ghiaasi, D. Vlastaras, M. Ashury, M. Hofer, Z. Xu & T. Zemen, "Real-Time Vehicular Channel Emulator for Future Conformance Tests of Wireless ITS Modems" in *Proc. of 10th European Conference on Antennas and Propagation (EuCAP)*, IEEE, Davos, Switzerland, p. 1–5, April 2016.

[7] M. Nilsson, D. Vlastaras, T. Abbas, B. Bergqvist & F. Tufvesson, "On Multilink Shadowing Effects in Measured V2V Channels on Highway" in *Proc. of 9th European Conference on Antennas and Propagation (EuCAP)*, IEEE, Lisbon, Portugal, p. 1–5, May 2015.

Acknowledgements

First and foremost, I would like to thank my supervisor, Prof. Fredrik Tufvesson, for his support and guidance during my doctoral studies. Without his valuable feedback and insightful discussions I would not have been able to complete this journey. Special thanks go also to my former colleague, Dr. Taimoor Abbas, who was of great assistance in the beginning of my studies. I would also like to thank my co-supervisor, Prof. Ove Edfors, for his input and funny stories during lunches.

My sincere gratitude goes to the people that have been feeding me and putting a roof over my head for the last few years, the Swedish tax payers, which through the Swedish Governmental Agency for Innovation Systems (VINNOVA) have been financing me in the FFI project Wireless Communication in Automotive Environment (WCAE).

My special thanks go to my colleagues and collaborators in Sweden and abroad for their time and effort: Steffen Malkowsky, Carl Gustafson, Mikael Nilsson, Russ Whiton, Magnus Olbäck, Carmine Celozzi, Prof. Thomas Zemen, Dr. Golsa Ghiaasi, Markus Hofer and Dr. Zhinan Xu

I would also like to thank Volvo Car Corporation, Volvo Trucks, ACTIA Nordic, Kapsch TrafficCom and SP Technical Research Institute of Sweden for supplying vehicles and equipment required for our measurement campaigns.

My sincere thanks go to colleagues and administrative stuff at work: Christian Nelson, Erik Bengtsson, Jose Flordelis, Xuhong Li, Saeedeh Moloudi, Dr. Nafiseh Mazloum, Dr. Rohit Chandra, Atif Yaqoob, Dr. Ghassan Dahman, Assoc. Prof. Fredrik Rusek, Assoc. Prof. Anders J Johansson, Assoc. Prof. Michael Lentmaier, Assoc. Prof. Liang Liu, Prof. Daniel Sjöberg, Prof. Buon Kiong Lau, Anne Andersson, Marianne Svensson, Pia Bruhn, Dorthe Jensen, Elisabeth Nordström, Göran Jönsson, Martin Nilsson, Josef Wajnblom, Per-Henrik Rasmussen, Peter Polfeldt, and Jessica Nilsson.

I would like to dedicate a whole paragraph to Zach, Ivaylo, Muris and João because they deserve it. Without them the corridors would not be the same. Countless hours spent on fika and philosophizing on elaborated problems we

didn't know we have is one of the requirements if one wants to survive the hurdles of doctoral studies.

Μαμά και μπαμπά, έφτασε τελικά ο καιρός μετά από 25 χρόνια να τελειώσω το σχολείο, καιρός ήταν. Όπως και να έχει δεν θα είχα φτάσει εδώ που είμαι σήμερα αν δεν είχατε κάνει τις επιλογές που κάνατε για εμένα, και για αυτό είμαι ευγνώμων!

Cristina, tu foste o motivo pelo qual consegui atingir os meus objetivos até ao momento atual. Obrigado por me fazeres ter os pés assentes na terra (exepto quando estou a pilotar aviões), e por partilhares esta jornada, um pouco atribulada, comigo.

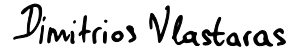

Dimitrios Vlastaras
Δημήτριος Βλαστάρας

List of Acronyms and Abbreviations

3GPP 3rd generation partnership project

ACF auto-correlation function

AOA angle of arrival

AOD angle of departure

ASA arrival angular spread

ASD departure angular spread

BS base station

BTP basic transport protocol

BU bad urban area

C2X car-to-anything

CAM cooperative awareness message

CAN-bus controller area network bus

CDC-ECM communications device class – ethernet control model

CDF cumulative distribution function

COST European cooperation in science and technology

CV constant velocity

DI static diffuse scatterer

DS delay spread

EM expectation maximization

ETSI European telecommunications standards institute

EuCAP European conference on antennas and propagation

FFI fordonsstrategisk forskning och innovation

GN GeoNetworking

GPS global positioning system

GSCM geometry-based stochastic channel model

GSM global system for mobile communications

Hi highway scenario

HT hilly terrain

IEEE institute of electrical and electronics engineers

InH indoor hotspot

ITS intelligent transportation systems

ITST international conference on ITS telecommunications

ITU international telecommunications union

ITU-R international telecommunications union radiocommunication sector

K K-factor

LOS line-of-sight

LS least squares

LT long term

MD mobile discrete scatterer

MIMO multiple-input multiple-output

MISO multiple-input single-output

MLE maximum likelihood estimation

MPC multi-path component

MS mobile station

NLOS non line-of-sight

NTP network time protocol

O2I outdoor-to-indoor

OLOS obstructed line-of-sight

OP opposite direction

P2P peer-to-peer

PDF probability density function

PDP power-delay profile

PER packer error rate

RA rural area

RF radio frequency

RMa rural macrocell

RMS root mean square

RMSE root-mean-square error

RSU road-side unit

Ru rural motorway scenario

RX receiver

SD static discrete scatterer

SDR software-defined radio

SF shadow fading

SISO single-input single-output

SM same direction

SMa suburban macrocell

ST short term

TDL tapped delay-line

TU typical urban area

TX transmitter

UDP user datagram protocol

UMa urban macrocell

UMi urban microcell

UMRR universal medium-range radar

USB universal serial bus

UTC coordinated universal time

V2I vehicle-to-infrastructure

V2V vehicle-to-vehicle

V2X vehicle-to-everything

VTC vehicular technology conference

WAVE wireless access in vehicular environments

WCAE wireless communication in vehicular environment

WGS84 world geodetic system 1984

WINNER wireless world initiative new radio

WiVeC international symposium on wireless vehicular communications

WSSUS wide-sense stationary uncorrelated-scattering

XPR cross-polarization ratio

Contents

Chapter 1

Introduction

Humans and other animals have used communication for millions of years as a tool to increase awareness of their environment and resolve conflicts. Communication can similarly be used in a vehicular context to increase situational awareness and avoid accidents.

Since the invention of the first car available to the masses, the 1908 Ford Model T, vehicles have been involved in accidents. The number of cars driving on public streets throughout the years has been increasing as the number of fatal accidents has been decreasing, as it can be seen in Fig. 1.1. This is partially due to enforced legislation and technological advances. In the modern world, people have the need to get quickly and conveniently from A to B. Modern technology in recent years, e.g. through vehicular radars and other sensing mechanisms, has proven itself and prevented many accidents by predicting them. Hopefully with with wireless communication this trend will continue and fatal accidents will eventually vanish not just by being predicted but avoided altogether.

This introduction starts by explaining what vehicular communication is, it continues by explaining what wireless channel models are, and finally an overview of the thesis is given.

1.1 Vehicular Communication

Vehicular communication falls within the broader group of Intelligent Transportation Systems (ITS) as it can be seen in Fig. 1.2. Intelligent Transportation Systems can be defined as a group of technological solutions in telematics designed to improve the safety and efficiency of terrestrial transportation.

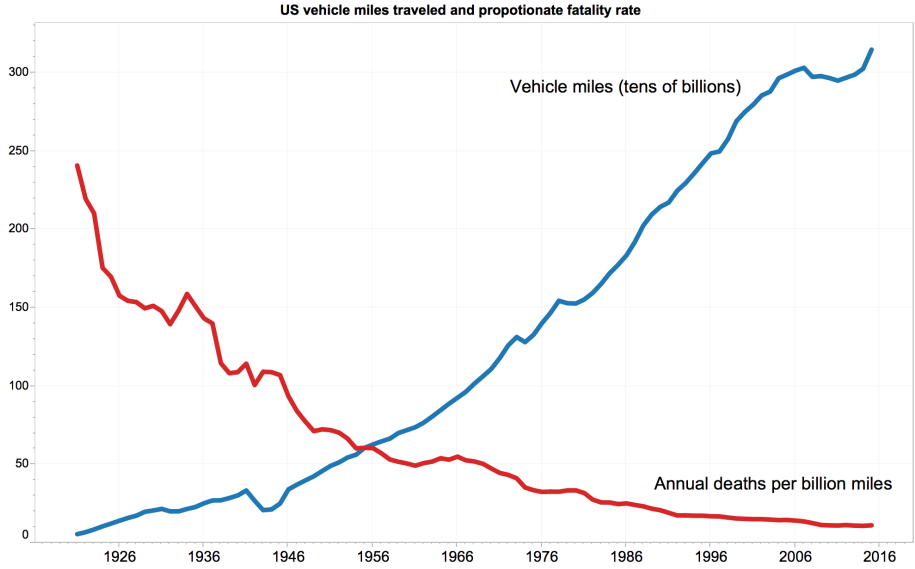

Figure 1.1: Annual US traffic fatalities per billion vehicle miles traveled (red) and miles traveled (blue) from 1921 to 2015. Data source: National Highway Traffic Safety Administration. Used under license: CC BY-SA 3.0. ©Dennis Bratland.

Vehicular communication can be divided in two different groups: vehicle-to-vehicle (V2V) and vehicle-to-infrastructure (V2I) communication. Both groups are some times referred to as vehicle-to-everything (V2X). This thesis touches upon both groups with focus on V2V communication. However, the road side unit (RSU) part of the thesis, which is covered in chapter 2, is a mixture of V2V and V2I. The reason is that a RSU is part of the infrastructure, not a vehicle. However in this case the RSU emulates a vehicle from the viewpoint of another vehicle, thus is falls within both groups.

V2V communication has been introduced, and standardized in different standards across the world. Both the European standard, ITS-G5, and its American counterpart, WAVE, are based on the IEEE 802.11p [1] amendment to the IEEE 802.11 [2] standard. Those standards define, amongst other, procedures to broadcast the position and velocity vectors of each individual vehicle so other nearby vehicles can collect this information and use it for safety purposes and enhance the driving experience. The functionality is achieved by exchanging cooperative road safety, traffic efficiency and other location aware-

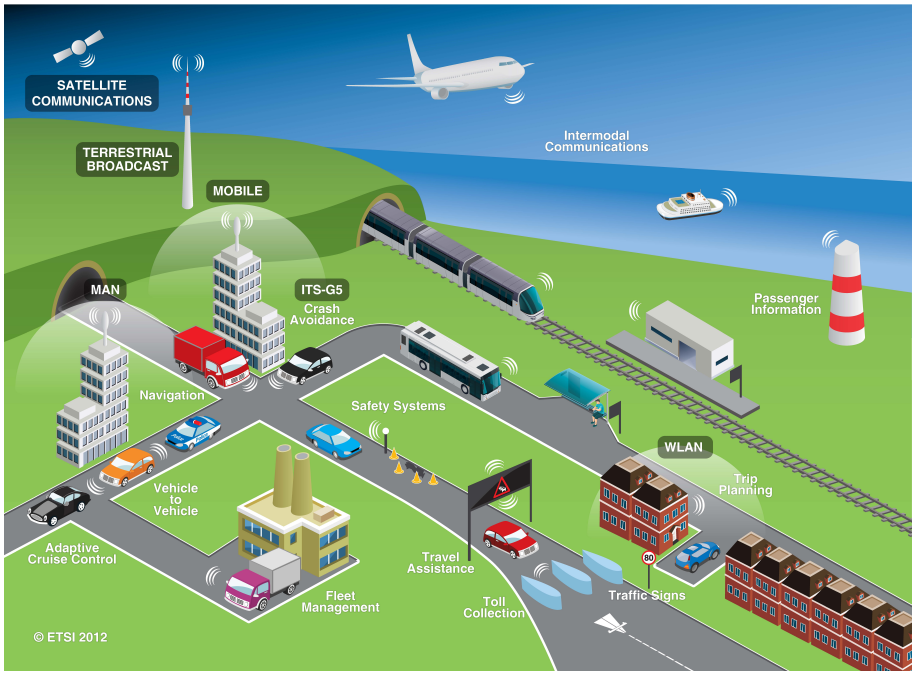

Figure 1.2: Intelligent Transportation Systems (ITS) is a broader group of technologies. Vehicular communication is a part of it. Image used with permission from ETSI.

ness messages in an ad-hoc configuration in the 5.9 GHz band [3–5]. V2V is extremely beneficial in the situations where the visual line-of-sight (LOS) is obstructed by buildings or other taller vehicles. Those scenarios are defined as obstructed line-of-sight (OLOS) and non line-of-sight (NLOS). OLOS is defined as the case where a sizable obstacle, e.g. a truck, is placed between the transmitter (TX) and the receiver (RX). NLOS is when a larger object completely blocks the line-of-sight, e.g. a building. This thesis contributes to solutions trying to mitigate problems that arise from those scenarios.

1.2 Wireless Channel Models

In communication the medium over which information is being transferred is called the channel. In wireless communication in particular the channel is physical environment that lies between the transmitter and the receiver. This

can be the molecules in the air, the ground, buildings, trees, and other kinds of objects. It is important for this wireless channel to be well understood in order to improve the performance of wireless transceivers.

An attempt to describe the channel and try to predict the channel gain is Ray Tracing. Just as in computer graphics, ray tracing is a way of tracking beams of energy that interact with a simplified model of the environment. In wireless communication this can be achieved by solving Maxwell's equations for an environment whose object dimensions are much greater than the wavelength of the electromagnetic waves.

However, from a communication point of view, it is not needed to describe the channel in such a great detail. Citing Karedal *et al., any channel model is a compromise between simplicity and accuracy* [6]. As long as some statistic for the behavior of few characteristics of the channel is known then this could be good enough. This is specially important in vehicular communication where the channel is much more dynamic and deterministic answers cannot be given easily. This is where stochastic channel models come in handy. Stochastic channel models usually give some kind of statistic, e.g. a distribution, mean and variance, for a specific environment, for one or more channel parameters, e.g. path loss, large-scale fading, small-scale fading, shadowing loss, Doppler spread, Delay spread, cross-correlations, etc...

In the sections below a few select cellular and vehicular channels models are being presented and discussed.

1.2.1 Cellular Channel Models

Cellular communication is significantly different from vehicular communication. The biggest difference is the base station. In cellular communication there is a base station that is usually placed at a high altitude, where it has a greater chance to be in the line-of-sight of another terminal or good scattering points. In vehicular environments, the communication is peer-to-peer (P2P) and thus no base station is involved. This increases the chance of non line-of-sight and obstructed line-of-sight scenarios. Vehicular models have to be constructed in such a way that the specific needs of such an environment are being addressed.

The cellular channel models covered in this section are based on ones used in real life for cellular communication around the world, being presented in chronological order.

The Okumura–Hata Model

The Okumura–Hata model is based on extensive measurements that were done by Okumura *et al.* [7] in 1968 in Japan. Those measurements were later adapted

for computer simulations by Hata [8] in 1980.

The model provides an empirical formula for propagation loss. The propagation loss in an urban area is presented in the following form: $A + B \log_{10} R$, where A and B are frequency and antenna height functions and R is the distance between the base station and the mobile station. The model is valid for the frequency range 100–1500 MHz, distance 1–20 km, base station height 30–200 m and mobile station height 1–10 m. Corrections are provided for suburban and open areas. The values of functions A and B can be taken from tables that can be found in [8].

The COST 231–Walfisch–Ikegami Model

The COST action 231 has resulted to two models, the COST 231–Hata and the COST 231–Walfisch–Ikegami model. They are both found in the COST 231 final report [9]. Those are some of the most used path-loss models in mobile communication, recommended by the International Telecommunications Union (ITU) [10] and the European Telecommunications Standards Institute (ETSI) [11].

The COST 231–Hata model is an extension of the Okumura–Hata [8] model to a higher frequency range, 1500–2000 MHz instead of 100–1500 MHz. This model is used for larger distances, at least a few kilometers. However, the model was not adequate for shorter distances and thus the COST 231–Walfisch–Ikegami was developed.

The COST 231–Walfisch–Ikegami model brings together the works of Walfisch and Bertoni, and Ikegami. It has three main components: A free space component, a component for propagation over roofs, and finally a component for propagation inside streets. For the LOS case the path-loss model can be expressed as

$$L_p\,[\mathrm{dB}] \quad = \quad 42.6 + 26 \log_{10}(d) + 20 \log_{10}(f)\,, \tag{1.1}$$

where d [km] is distance between the base station and the mobile station, and f [MHz] is the carrier frequency. The COST 231–Walfisch–Ikegami path-loss model for the NLOS case can be expressed as

$$L_p\,[\mathrm{dB}] \quad = \quad \begin{cases} L_0\,[\mathrm{dB}] + L_{msd}\,[\mathrm{dB}] + L_{rts}\,[\mathrm{dB}] & , \quad L_{msd} + L_{rts} > 0 \\ L_0\,[\mathrm{dB}] & , \quad L_{msd} + L_{rts} \leq 0\,. \end{cases} \tag{1.2}$$

The free space component, provided by Ikegami, considers the general attenuation from the base station to the mobile station without taking into account buildings or any other obstacles. It is given by

$$L_0\,[\mathrm{dB}] \quad = \quad 32.44 + 20 \log_{10}(d) + 20 \log_{10}(f)\,, \tag{1.3}$$

where d [km] is the distance between the base station and the mobile station, and f [MHz] is the carrier frequency.

The rooftop component, based on works by Walfisch and Bertoni, considers the attenuation provided by the diffraction that occurs at the rooftop edges until the street of the mobile station. It is given by

$$\begin{aligned} L_{msd}\,[\mathrm{dB}] &= L_{bsh}\,[\mathrm{dB}] + k_a + k_d \log_{10}(d) + k_f \log_{10}(f) \\ &- 9 \log_{10}(w_B)\,, \end{aligned} \tag{1.4}$$

$$L_{bsh}\,[\mathrm{dB}] = \begin{cases} -18 \log_{10}(h_b - H_B + 1) & , \quad h_b > H_B \\ 0 & , \quad h_b \leq H_B \end{cases}, \tag{1.5}$$

where d [km] is the distance between the base station and the mobile station, f [MHz] is the frequency, w_B [m] is the building width, h_b [m] is the base station height, and H_B [m] is the building height. The attenuation factor h_a, distance factor h_d, and frequency factor k_f can be found in literature about the COST 231–Walfisch–Ikegami model [9, 12, 13], and they vary depending on scenario.

Finally, the street component, based on works by Ikegami, considers the propagation in-between the buildings until the mobile station, that generates a canyon effect but doesn't consider wave guiding. It is given by

$$\begin{aligned} L_{rts}\,[\mathrm{dB}] &= -16.9 - 10 \log_{10}(w_s) + 10 \log_{10}(f) \\ &+ 20 \log_{10}(\Delta h_m) + L_{ori}\,[\mathrm{dB}]\,, \end{aligned} \tag{1.6}$$

$$L_{ori}\,[\mathrm{dB}] = \begin{cases} -10.0 + 0.354\phi & , \quad 0^\circ \leq \phi < 35^\circ \\ 2.5 + 0.075(\phi - 35) & , \quad 35^\circ \leq \phi < 55^\circ \\ 4.0 - 0.114(\phi - 55) & , \quad 55^\circ \leq \phi \leq 90^\circ \end{cases}, \tag{1.7}$$

where $\Delta h_m[\mathrm{m}] = H_B - h_m$, f [MHz] is the frequency, w_s [m] is the street width, H_B [m] is the building height, h_m [m] is the mobile station height, and ϕ is the angle of arrival of the signal relative to the building walls which are perpendicular to the street.

A more comprehensive overview of the COST 231–Walfisch–Ikegami model can be found in [12].

The COST 207 GSM Model

The COST action 207 model [14], mostly used in GSM communications, was created to describe four different environments: rural area (RA), typical urban

area (TU), bad urban area (BU), and hilly terrain (HT). It provides normalized scattering functions and amplitude statistics for these environments. The power-delay profile (PDP) for the rural area is given by

$$P_h(\tau) = \begin{cases} e^{-9.2\tau/\mu s} & , \quad 0 < \tau < 0.7\,\mu s \\ 0 & , \quad \text{otherwise} \end{cases} , \tag{1.8}$$

for the typical urban area is given by

$$P_h(\tau) = \begin{cases} e^{-\tau/\mu s} & , \quad 0 < \tau < 7\,\mu s \\ 0 & , \quad \text{otherwise} \end{cases} , \tag{1.9}$$

for the bad urban area is given by

$$P_h(\tau) = \begin{cases} e^{-\tau/\mu s} & , \quad 0 < \tau < 5\,\mu s \\ 0.5e^{5-\tau/\mu s} & , \quad 5 < \tau < 10\,\mu s \\ 0 & , \quad \text{otherwise} \end{cases} , \tag{1.10}$$

and for the hilly terrain is given by

$$P_h(\tau) = \begin{cases} e^{-3.5\tau/\mu s} & , \quad 0 < \tau < 2\,\mu s \\ 0.1e^{15-\tau/\mu s} & , \quad 15 < \tau < 20\,\mu s \\ 0 & , \quad \text{otherwise} \end{cases} . \tag{1.11}$$

When the model is realized as a tapped delay-line (TDL), each tap with index i has a Doppler spectrum $P_s(\nu, \tau_i)$. There are four types of Doppler spectra defined in the model. For delays $\tau_i \leq 0.5\mu s$ the classical (CLASS) Jakes' Doppler spectrum is being used and it is given by

$$P_s(\nu, \tau_i) = \frac{A}{\sqrt{1-\left(\frac{\nu}{\nu_{\max}}\right)^2}} \quad , \quad \nu \in [-\nu_{\max}, \nu_{\max}] \ . \tag{1.12}$$

For delays in the interval $0.5\mu s \leq \tau_i \leq 2\mu s$ the sum of two Gaussian functions (GAUS1) is used and is given by

$$\begin{aligned} P_s(\nu, \tau_i) &= G(A, -0.8\nu_{\max}, 0.05\nu_{\max}) + G(A_1, 0.4\nu_{\max}, 0.1\nu_{\max}) \\ A_1 &= A - 10\,\text{dB} . \end{aligned} \tag{1.13}$$

For delays higher than $\tau \geq 2\,\mu s$ another sum of two Gaussian functions (GAUS2) is being used and is given by

$$\begin{aligned} P_s(\nu, \tau_i) &= G(B, 0.7\nu_{\max}, 0.1\nu_{\max}) + G(B_1, -0.4\nu_{\max}, 0.15\nu_{\max}) \\ B_1 &= B - 15\,\text{dB} . \end{aligned} \tag{1.14}$$

For the shortest path of the model for propagation in rural areas the classical Jakes' Doppler spectrum with one direct path is being used (RICE). It is equivalent to the CLASS Doppler spectrum, but with an impulse at the Doppler shift corresponding to the line-of-sight component. It is given by

$$\begin{aligned} P_s(\nu,\tau_i) &= \frac{0.41}{2\pi\nu_{\max}\sqrt{1-\left(\frac{\nu}{\nu_{\max}}\right)^2}} \\ &+ 0.91\delta(\nu-0.7\nu_{\max}) \quad , \quad \nu\in[-\nu_{\max},\nu_{\max}] \ . \end{aligned} \tag{1.15}$$

The Gaussian function G is given by

$$G(A,\nu_1,\nu_2) = Ae^{-\frac{(\nu-\nu_1)^2}{2\nu_2^2}} , \tag{1.16}$$

where A is a normalization constant selected in such a way that

$$\int P_s(\nu,\tau_i)d\nu = 1. \tag{1.17}$$

Parameterization for delay tap number, delay, power and Doppler category for various environments can be found in table format in literature about the COST 207 model [13, 14].

The ITU–R Models

The International Telecommunications Union radiocommunication sector (ITU–R) developed a set of channel models meant to be for third generation (3G) cellular systems [13, 15]. The models specify three environments: indoor, pedestrian and vehicular. Two channels, A and B, are specified for each of the environments. Channel A is the low delay spread case and channel B is the high delay spread case. The models are available as a tapped delay-line implementations. The amplitudes follow a Rayleigh distribution. The Doppler spectrum is uniformly distributed in the interval $[-\nu_{\max},\nu_{\max}]$ for the indoor environment and distributed according to the classical Jakes' Doppler spectrum for the pedestrian and vehicular environments. It's worth mentioning that the channel models intended for the vehicular environment assume high base station antennas and are not suitable for V2V. The ITU model specifies path loss for the indoor environment as

$$L_p\,[\mathrm{dB}] = 37 + 30\log_{10} d + 18.3 N_{\mathrm{floor}}^{\frac{N_{\mathrm{floor}}+2}{N_{\mathrm{floor}}+1}-0.46} , \tag{1.18}$$

for the pedestrian environment as

$$L_p\,[\mathrm{dB}] = 40\log_{10} d + 30\log_{10} f_c + 49\,, \tag{1.19}$$

and for the vehicular environment as

$$\begin{aligned} L_p\,[\mathrm{dB}] &= 40(1-4\cdot 10^{-3}\Delta h_b)\log_{10} d \\ &- 18\log_{10}\Delta h_b + 21\log_{10} f_c + 80\,, \end{aligned} \tag{1.20}$$

where d [km] is the distance, f_c [MHz] is the carrier frequency, and Δh_b is the base station height measured from the rooftop level. Δh_b must be within the interval $\in [0, 50]$ m for the model to be valid.

Log-normal shadowing is imposed for all three environments. The standard deviation is 12 dB for the indoor environment and 10 dB for the vehicular and pedestrian environments. The autocorrelation function (ACF) of the shadowing is assumed to be exponential and it is defined as

$$ACF(\Delta x) = e^{\frac{-\ln(2)|\Delta x|}{d_{\mathrm{corr}}}}\,, \tag{1.21}$$

where d_{corr} is the decorrelation distance and is only defined for the vehicular environment as 20 m. An outdoor-to-indoor case is defined for the pedestrian environment. The additional loss due to the building walls in this case is modeled as $\sim \mathcal{N}(12\,\mathrm{dB}, 8^2\,\mathrm{dB})$.

Tapped delay-line implementations of the ITU–R models, including delay tap number, delay and received power, can be found in table format in ITU–R model literature [13, 15].

The 3GPP Spatial Channel Model

The 3GPP and 3GPP2 are industry alliances between groups of telecommunications associations formed to standardize third generation (3G) mobile phone systems. However, they have also been involved in the standardization of fourth (4G) and fifth (5G) generation mobile phone systems. These alliances have developed a channel model for the evaluation of multiple antenna systems [16]. The channel model is compatible with channels of bandwidth ≤ 5 MHz. The model is defined for three different environments: urban microcells, urban macrocells, and suburban macrocells. As hinted by the model's name, it's a mix of geometrical and stochastic modeling.

The models define amongst other options: path loss, narrowband parameters, wideband parameters for the macrocell and microcell environments, and generation of fast-fading coefficients. For the suburban and urban macrocell environments the path loss is given by

$$\begin{aligned} L_p\,[\mathrm{dB}] &= (44.9 - 6.55\log_{10}(h_{\mathrm{BS}}))\log_{10}\left(\frac{d}{1000}\right) \\ &+ 45.5 + (35.46 - 1.1 h_{\mathrm{MS}})\log_{10}(f_c) \\ &- 13.82\log_{10}(h_{\mathrm{MS}}) + 0.7 h_{\mathrm{MS}} + C\,, \end{aligned} \tag{1.22}$$

and for the urban microcell environment the path loss is given by

$$L_p\,[\mathrm{dB}] \quad = \quad -55.9 + 38\log_{10}(d) + \left(24.5 + \frac{f_c}{616.67}\right)\log_{10}(f_c)\,, \quad (1.23)$$

where h_{BS} [m] is the base station antenna height, h_{MS} [m] is the mobile station antenna height, f_c [MHz] is the carrier frequency, d [m] is the distance between the base station and the mobile station and has to be $\geq 35\,\mathrm{m}$, and C is a constant defined as $C = 0\,\mathrm{dB}$ for the suburban macrocell environment and $C = 3\,\mathrm{dB}$ for the urban macrocell environment. More details about the 3GPP spatial channel model can be found in [13, 16].

The ITU–Advanced Channel Model

The final channel model for cellular communications overviewed in this thesis is the ITU–advanced channel model [17]. The ITU modeling method is very similar to the one found in the 3GPP model. Most of the measurement campaigns were done within the European projects WINNER and WINNER2. A very large range of scenarios is covered, and thus this overview is short and brief.

Five deployment scenarios are covered by the model, they are: indoor hotspot (InH), urban microcell (UMi), urban macrocell (UMa), suburban macrocell (SMa), and rural macrocell (RMa). Whether a mobile station is LOS or NLOS is decided by a probability density function (PDF) which is specific to each scenario. Path loss for each scenario is provided by the model and it varies with whether a mobile station is LOS or NLOS. The environment layout also matters for some scenarios, such as UMi NLOS and UMi outdoors-to-indoors (O2I). Other options that are given by the model and vary with scenario are: delay spread (DS), angle-of-departure (AOD) spread, angle-of-arrival (AOA) spread, shadow fading (SF), K-factor (K), cross-correlations, delay distribution, AOD and AOA distributions, delay scaling parameter, cross-polarization ratio (XPR), number of clusters, number of rays, cluster departure angular spread (ASD), cluster arrival angular spread (ASA), per cluster shadowing standard deviation, and correlation distance. More details about the ITU–Advanced Channel model can be found in [13, 17].

1.2.2 Vehicular Channel Models

In the previous section, a few cellular channel models were briefly introduced. Even though many cellular channel models include vehicular environments in their descriptions, the base station assumption is still present, no matter the

frequency or whether the model is designed for single or multiple antenna systems. In vehicular environments high speeds are usually encountered. This often means that the wide-sense stationary uncorrelated scattering (WSSUS) assumption is violated [6]. Also the Doppler and delay spreads are increased [18]. It is thus important to characterize wireless communication in vehicular environments and tailor channel models specifically for this case.

GSCM MIMO Channel Model for V2V

The geometry-based stochastic (GSCM) multiple-input multiple-output (MIMO) channel model by Karedal *et al.* was born as a need to model vehicle-to-vehicle communication in rural and highway environments using the IEEE 802.11p standard. Vehicular communication, in constrast to cellular communication, does not depend on a base station. The multipath components stay near the ground. This leads to destructive interferance fading, a more dynamic channel due to the nature of vehicles and an environment rich in dynamic and static scattering. The overview of the model will closely follow [6].

The model was constructed for a center frequency of 5.2 GHz due to regulatory restrictions during the measurement campaign. However, this band was deemed to be close enough to 5.9 GHz of IEEE 802.11p for no significant differences to be expected in the propagation environment.

As mentioned earlier, the model covers the rural motorway (Ru) and highway (Hi) scenarios in V2V communications. The rural environment is characterized by fields on either side of the road with some sparse residential houses, farm houses, road signs and little to no traffic. The highway environment is quite similar to rural or suburban environments where the roadside either consists of fields or noise barriers. There are road signs and low commercial buildings. Near exist ramps of the highway, strong static scattering points are to be expected, otherwise to be scarce along the route. The model describes traffic traveling both the same (SM) and opposite (OP) directions.

It is worth to mention that the model does not rely on the WSSUS assumption since discrete components typically move through many delay bins during vehicular communication.

The basic idea of GSCMs is to place scatterers in the environment according to certain statistical properties. Thus the model is comprised of three different kinds of scatterers: mobile discrete (MD), static discrete (SD), and static diffuse (DI). The assumed environment where the scatterers are placed is a N_{lanes}-lane road with a dividing barrier in the middle. Only two dimensions are considered by the model. The width of the road is assigned the y-coordinate and the length of the road is assigned the x-coordinate. The road geometry can be seen in Fig. 1.3.

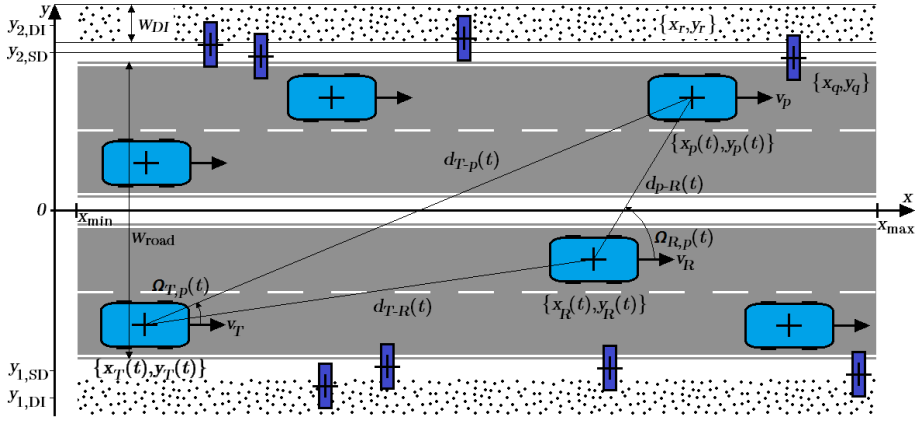

Figure 1.3: The road geometry considered in the geometry-based stochastic MIMO model for V2V by Karedal *et al.* The transmitter is at coordinates $\{x_T(t), y_T(t)\}$ moving with velocity v_T while the receiver is at coordinates $\{x_R(t), y_R(t)\}$ moving with velocity v_R. Other vehicles are mobile discrete (MD) scatterers at coordinates $\{x_p(t), y_p(t)\}$ moving with velocity v_p. Road signs and other similar features are are static discrete (SD) scatterers at coordinates $\{x_q, y_q\}$. The dots are static diffuse (DI) scatterers at coordinates $\{x_r, y_r\}$.

The MD scatterers are other vehicles on the road with coordinates $\{x_p(t), y_p(t)\}$. Their y-coordinates are modeled by a uniform discrete PDF where the number of possible outcomes equals to N_{lanes}. Their *initial* x-coordinates are modeled by a continuous uniform distribution over the length of the road strip, i.e. $x_{p,0} \sim \mathcal{U}(x_{\min}, x_{\max})$ where $x_{\min}$ and $x_{\max}$ are the limits of the road. Each MD scatterer is assigned a constant velocity along the x-axis given by a truncated Gaussian distribution in order to avoid negative and extremely high velocities.

The SD scatterers are road signs and other significant scattering points in the sides and barrier of the road with coordinates $\{x_q, y_q\}$. Their y-coordinates are modeled as $y_q \sim \mathcal{N}(y_{1,\text{SD}}, \sigma_{y,\text{SD}})$ or $y_q \sim \mathcal{N}(y_{2,\text{SD}}, \sigma_{y,\text{SD}})$ depending on which side of the road they reside on, where σ is the standard deviation. SD scatterers may also be placed in the barrier in the middle of the road and correspond overhead road signs. Their x-coordinates are modeled as $x_q \sim \mathcal{U}(x_{\min}, x_{\max})$.

The DI scatterers are other elements in the side of the road with coordinates $\{x_r, y_r\}$. Their y-coordinates are uniformly distributed over the intervals $y_r \sim$

$\mathcal{U}(y_{1,\mathrm{DI}} - W_{\mathrm{DI}}/2, y_{1,\mathrm{DI}} + W_{\mathrm{DI}}/2)$ or $y_r \sim \mathcal{U}(y_{2,\mathrm{DI}} - W_{\mathrm{DI}}/2, y_{2,\mathrm{DI}} + W_{\mathrm{DI}}/2)$, where W_{DI} is the width of the DI scatterer field on each side of the road. Their x-coordinates are modeled as $x_r \sim \mathcal{U}(x_{\min}, x_{\max})$.

The model provides the bi-directional, time-variant, impulse response of the channel as contributions of N scatterers. The impulse response is divided into four parts in agreement with performed measurements, given by

$$\begin{aligned} h(t,\tau) &= h_{\mathrm{LOS}}(t,\tau) + \sum_{p=1}^{P} h_{\mathrm{MD}}(t,\tau_p) \\ &+ \sum_{q=1}^{Q} h_{\mathrm{SD}}(t,\tau_q) + \sum_{r=1}^{R} h_{\mathrm{DI}}(t,\tau_r)\,, \end{aligned} \tag{1.24}$$

where P is the number of MD scatterers, Q is the number of SD scatterers and R is the number of DI scatterers.

The complex path amplitude α_p for both SD and MD scatterers is modeled as fading. It is divided in a deterministic distance decaying and a stochastic part, i.e.

$$\alpha_p(d_p) = g_{\mathrm{S},p} e^{j\phi_p} G_{0,p}^{1/2} \left(\frac{d_{\mathrm{ref}}}{d_p} \right)^{n_p/2}, \tag{1.25}$$

where $d_p = d_{T\to p} + d_{p\to R}$, $G_{0,p}$ is the received power at a reference distance d_{ref}, n_p is the path-loss exponent and $g_{S,p}$ is the real-valued, slowly varying, stochastic amplitude gain of the scatterer. The random phase shift is modeled uniformly over the interval $[0, 2\pi)$.

For the LOS component the same model as for the MD and SD components has been selected. This is due to ground reflections which cannot be resolved from the true LOS due to relatively low resolution in the delay domain. Thus the same equation as (1.25) has been used, with the subscript p replaced by LOS.

For DI scatterers, the complex path amplitude has been modeled as

$$\alpha_r = G_{0,\mathrm{DI}}^{1/2} c_r \left(\frac{d_{\mathrm{ref}}}{d_{T\to p} \times d_{p\to R}} \right)^{n_{\mathrm{DI}}/2}, \tag{1.26}$$

where c_r is zero-mean complex Gaussian distributed according to observations, n_{DI} is the path-loss exponent and $G_{0,\mathrm{DI}}$ is the reference power which is the same for all DI scatterers.

Complete parametrization of the model for both rural and highway environments, LOS, MD, SD and DI parts of the impulse response, together with more information and implementation recipe of the model can be found in [6].

Intersection Model for V2V

While the GSCM MIMO V2V model by Karedal *et al.* covers the rural and highway environments, it does not cover the intersection environment. Abbas *et al.* in [19] validate a reference non line-of-sight path-loss and fading channel model for vehicle-to-vehicle communication at 5.9 GHz by Mangel *et al.* [20] with independent and realistic measurement data. The model fits well, with a few exceptions, to the measured data. An additional parameter that depends on the properties and number of available scatterers in a particular intersection is introduced in the model so that it can be made more general. The reference model is named *VirtualSource11p* and is a modified version of a path-loss model for cellular communications proposed in [21].

The path-loss equation of the reference model is given by

$$\begin{aligned} L_p(d_r, d_t, w_r, x_t, i_s)\,[\mathrm{dB}] &= C + i_s L_{\mathrm{SU}} \\ &+ \begin{cases} 10\log_{10}\left(\left(\frac{d_t^{E_\mathrm{T}}}{(x_t w_r)^{E_\mathrm{S}}}\frac{4\pi d_r}{\lambda}\right)^{E_\mathrm{L}}\right) & , \quad d_r \le d_b \\ 10\log_{10}\left(\left(\frac{d_t^{E_\mathrm{T}}}{(x_t w_r)^{E_\mathrm{S}}}\frac{4\pi d_r^2}{\lambda d_b}\right)^{E_\mathrm{L}}\right) & , \quad d_r > d_b \end{cases} , \end{aligned} \tag{1.27}$$

where d_t and d_r [m] denote the distance from the intersection center to the TX and RX respectively, w_r [m] is the width of the RX street, x_t [m] is the distance from the TX to the wall, C [dB] is the curve shift, L_{SU} [dB] is the suburban loss, i_s is the urban/suburban loss factor, E_L is the loss exponent, E_S is the street exponent, E_T is the TX distance exponent and d_b [m] is the break-even distance. Given a known transmitted power $P_{\mathrm{TX}}(d)$ and the fact that the path loss for a certain distance can be calculated by the model, the received power $P_{\mathrm{RX}}(d)$ can by calculated by

$$P_{\mathrm{RX}}(d)\,[\mathrm{dBm}] = P_{\mathrm{TX}}(d) - L_s + G_a - L_p(d_r, d_t, w_r, x_t, i_s)\,, \tag{1.28}$$

where L_s is the system loss and G_a is the combined TX–RX antenna gain.

After validation of the NLOS model, it is found that the model fits well with one exception. That is the case where strong reflections from metallic window structures are present in the street intersection. To tackle this problem, Abbas *et al.* propose the addition of another intersection depended gain parameter G_{ID} to equation (1.27). However, due to the lack of measurement data this parameter is not estimated. Otherwise complete model parametrization can be found in table format in [19].

Diffraction Model for V2V

Another important scenario in vehicular communication is when a big obstacle, e.g. a truck, is blocking the communication between two vehicles, e.g. two cars. Inconveniently, scenarios like this correlate largely with the use cases with the smallest margin for packet error due to high speeds, and often, heavy traffic density. It is thus important to investigate and model such scenarios. A model for power contributions around a truck due to diffraction [22] is one of the contributions of this thesis. The model is thoroughly described in chapter 4.

1.3 Thesis Overview

In chapter 2, a road side unit (RSU) that has been constructed and evaluated for integrating older vehicles without wireless communication with newer vehicles using wireless communication is described. Older vehicles are being detected using a universal medium-range radar and their position and velocity vectors are broadcasted wirelessly to newer vehicles. Tests have been performed by using the system in parallel with wireless enabled vehicles. Accuracy tests have been performed on the system and Kalman filtering has been applied to improve the accuracy even further. Chapter 2 is based on the following publications:

- D. Vlastaras, T. Abbas, D. Leston & F. Tufvesson, "Vehicle Detection through Wireless Vehicular Communication" in *EURASIP Journal on Wireless Communications and Networking*, p. 146–153, September 2014.
- D. Vlastaras, T. Abbas, D. Leston & F. Tufvesson, "Universal Medium Range Radar and IEEE 802.11p Modem Solution for Integrated Traffic Safety" in *Proc. of 13th International Conference on ITS Telecommunications (ITST)*, IEEE, p. 193–197, 2013.

Chapter 3 focuses on the OLOS scenario. A truck as an obstacle for wireless vehicular communication is being investigated. Real life measurements have been performed to characterize and model the wireless channel around the truck. The distance dependent path loss and additional shadowing loss due to the truck is analyzed through dynamic measurements. The large-scale fading, delay and Doppler spreads are characterized as a measure of the channel dispersion in the time and frequency domains. A model for power contributions due to diffraction around the truck has also been proposed and evaluated using the previously mentioned real life measurements. Chapter 3 is based on the following publications:

- D. Vlastaras & F. Tufvesson, "A model for power contributions from diffraction around a truck in Vehicle-to-Vehicle communications" in *Proc. of 15th International Conference on ITS Telecommunications (ITST)*, IEEE, Warsaw, Poland, May 2017. [Submitted]

- D. Vlastaras, T. Abbas, M. Nilsson, R. Whiton, M. Olbäck & F. Tufvesson, "Impact of a Truck as an Obstacle on Vehicle-to-Vehicle Communications in Rural and Highway Scenarios" in *Proc. of 6th International Symposium on Wireless Vehicular Communications (WiVeC)*, IEEE, Vancouver, Canada, p. 1–6, September 2014.

In the spirit of channel characterization and modeling, collaboration has been made with other authors to investigate further shadowing scenarios in vehicular communication. However, the following publication is not included in this thesis:

- M. Nilsson, D. Vlastaras, T. Abbas, B. Bergqvist & F. Tufvesson, "On Multilink Shadowing Effects in Measured V2V Channels on Highway" in *Proc. of 9th European Conference on Antennas and Propagation (EuCAP)*, IEEE, Lisbon, Portugal, p. 1–5, May 2015.

In chapter 4 a wireless channel emulator that has been constructed and evaluated is described. Modem manufacturers face a challenge when designing and implementing equipment for highly dynamic environments found in vehicular communication. For testing and evaluation real-life measurements with vehicles are required, which is often an expensive and slow process. The channel emulator proposed is designed and implemented using a software defined radio (SDR). The emulator together with the proposed test methodology enables quick on-bench evaluation of wireless modems. It may also be used to evaluate modem performance in various NLOS and OLOS scenarios. Chapter 4 is based on the following publication:

- D. Vlastaras, S. Malkowsky & F. Tufvesson, "Stress Test Of Vehicular Communication Transceivers Using Software Defined Radio" in *Proc. of 81st Vehicular Technology Conference (VTC)*, IEEE, Glasgow, Scotland, p. 1–4, May 2015.

The work described in chapter 4 has been extended in collaboration with other authors. However, the following publication which extends the work on the channel emulator, is not included in this thesis:

- G. Ghiaasi, D. Vlastaras, M. Ashury, M. Hofer, Z. Xu & T. Zemen, "Real-Time Vehicular Channel Emulator for Future Conformance Tests

of Wireless ITS Modems" in *Proc. of 10th European Conference on Antennas and Propagation (EuCAP)*, IEEE, Davos, Switzerland, p. 1–5, April 2016.

Finally, the thesis concludes with a brief summary of the aforementioned contributions and discussions of possible future work and ideas that could have been implemented.

Chapter 2

Old Vehicles and V2V

Both the European standard for ITS, ITS-G5, and its American counterpart, WAVE, are based on the IEEE 802.11p amendment to the IEEE 802.11 standard. Those standards define procedures to broadcast the position and velocity vectors of each individual vehicle so other nearby vehicles can collect this information and use it for safety purposes.

This technology comes with a problem during the implementation phase, as just a few of the vehicles in circulation will actually be equipped with on-board devices. This thesis focuses on addressing this problem by implementing a road side unit (RSU) that scans for vehicles and emulates Cooperative Awareness Messages (CAM) from them as if they had their own IEEE 802.11p on-board broadcasting modules [23]. This has been done using an IEEE 802.11p wireless modem together with a universal medium range radar (UMRR).

In the example portrayed in Fig. 2.1, the intelligent car in grey color, reaches an intersection where there is a known risk of collision with other vehicles due to the low visibility of the cars that approach from the right.

If all the vehicles in the example had a vehicle-to-everything (V2X) communication system, they would broadcast their position and velocity vectors and therefore the vehicle that aims to enter the main road would be aware of the risk of an accident. Nevertheless, a more realistic scenario would be that where the majority of the vehicles are not equipped with such a system.

However, the device described in this thesis can be placed in the intersection, monitoring all the vehicles that approach from the east and broadcasting their position and speed vectors as if they had their own on-board devices.

In the example above, the blue car is not equipped with a V2X communication system and it is driving at a high speed. The driver in the grey car, equipped with V2X, is not capable of seeing it since there are some trees block-

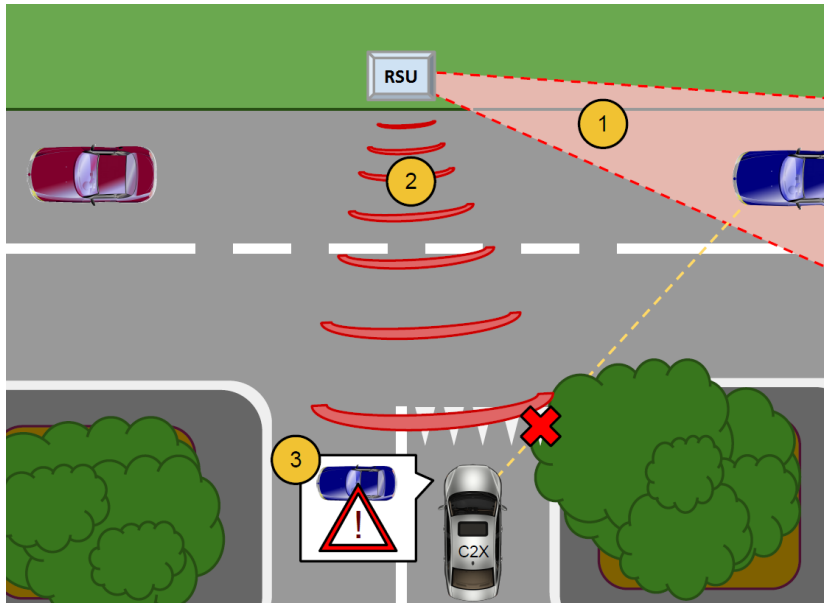

Figure 2.1: Possible traffic outcome where the line-of-sight of the grey vehicle towards the blue vehicle is blocked by some trees.

ing the line-of-sight (NLOS). Since the RSU is placed at the intersection, it will detect the blue car (1) and will transmit instant values of its position and speed vectors to the grey car (2). The V2X vehicle will then be notified about the approaching car and will alert the driver of the risk of collision if he or she decides to enter the main road (3).

The effect of intersections in vehicle-to-vehicle (V2V) communications has been widely studied in the past [19,24] and it has been concluded that most of the power contributions arise in the presence of line-of-sight (LOS). Therefore solutions that extend LOS, such as this road side unit, will play a major roll in the future of urban vehicular communications.

Traffic accidents, especially those taking place nearby or at intersections, have been studied during recent years and methods have been developed to be able to predict and avoid them [25–28]. However, a solution such as this RSU for detection of older vehicles in conjunction with automatic breaking systems or warning systems in newer vehicles is to the author's best knowledge new and has not been presented before. It can significantly improve the safety of terrestrial transportation by avoiding accidents rather than predicting them.

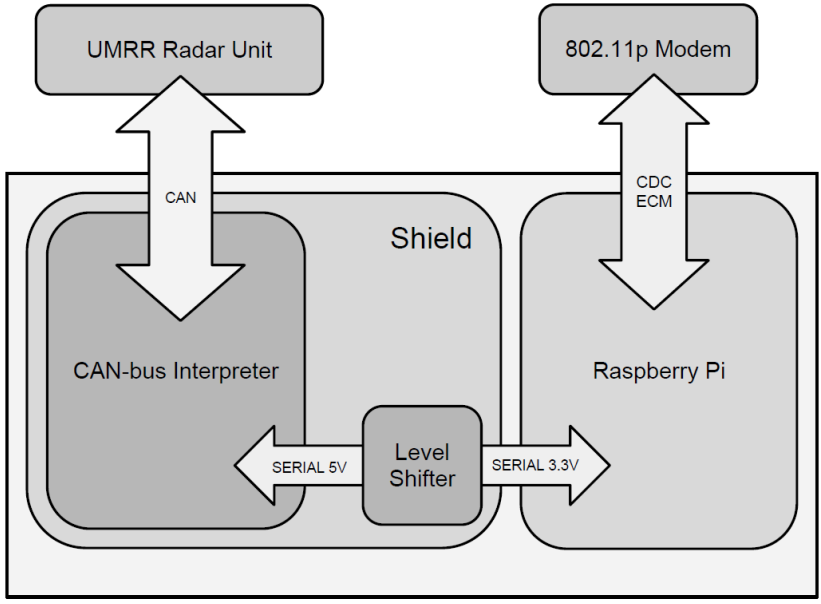

Figure 2.2: Block diagram of the system.

2.1 System Description

The road side unit consists of three main parts; a universal medium range radar unit, an IEEE 802.11p wireless modem and an embedded system that provides interfaces and intelligence to them both as seen in Fig. 2.2.

2.1.1 Universal Medium Range Radar

The radar has the capability of detecting vehicles up to 160 m of distance and with 25 cm of accuracy [29]. The technology utilizes microwaves in the 24 GHz band for detection of objects. It also incorporates smart functionality such as detection of vehicles that are solely moving in one direction, distinguishing between different kinds of vehicles and/or pedestrians and also providing their velocity and position vectors. This information is later being embedded into wireless frames and broadcasted to other vehicles.

This UMRR was designed for in-vehicle and traffic monitoring installations and it communicates with its surroundings over the CAN-bus protocol [30]. Therefore, the rest of the system has to implement the same protocol in order to send commands and receive responses to/from the UMRR.

2.1.2 IEEE 802.11p Wireless Modem

The modem incorporated in this RSU is a very basic one. It does not implement the full ITS-G5 standard, however it is transmitting and receiving information on the 5.9 GHz band using the IEEE 802.11p amendment.

The modem connects to the embedded system using the CDC-ECM[1] standard. Frames are sent to the modem over the UDP protocol. The only task that the modem has to perform is to open up those UDP datagrams and broadcast their payload wirelessly. The payload is expected to be frames according to the ITS-G5 standard.

2.1.3 Embedded System

The responsibility of the embedded system is to connect the UMRR unit with the IEEE 802.11p modem and run all the required software in order to meet the system requirements. The velocity and position vectors of each vehicle are reported using GeoNetworking (GN) [31], basic transport protocol (BTP) [32] and cooperative awareness message (CAM) [3] frames.

The embedded system is composed of two main parts; a CAN-bus shield and a Raspberry Pi[2] as seen in Fig. 2.3. The CAN-bus shield is responsible for the communication with the UMRR unit over CAN-bus and the Raspberry Pi is responsible for running the main algorithms and for the communication with the IEEE 802.11p modem over CDC-ECM.

The two parts communicate with each other over their respective RS-232 serial ports. The CAN-bus shield uses 5 V as reference for logic voltage while the Raspberry Pi uses 3.3 V. A voltage level shifter has been put in place to solve this problem.

2.2 Functional Tests

Two different kinds of tests were performed in Gothenburg, Sweden. The first test, communication test, was to determine whether the IEEE 802.11p Modem could successfully communicate with Volvo Drive C2X[3] equipment or not. The second test, verification test, was to determine whether the RSU ITS-G5 implementation followed the ITS-G5 specifications [3, 31, 32] by comparing frames from another ITS-G5 source, e.g. a Drive C2X Volvo car, to frames generated by the RSU.

[1] CDC-ECM is an implementation for Ethernet over USB.
[2] The Raspberry Pi is a credit-card-sized single-board computer.
[3] Drive C2X is a European integrated project on ITS deployment.

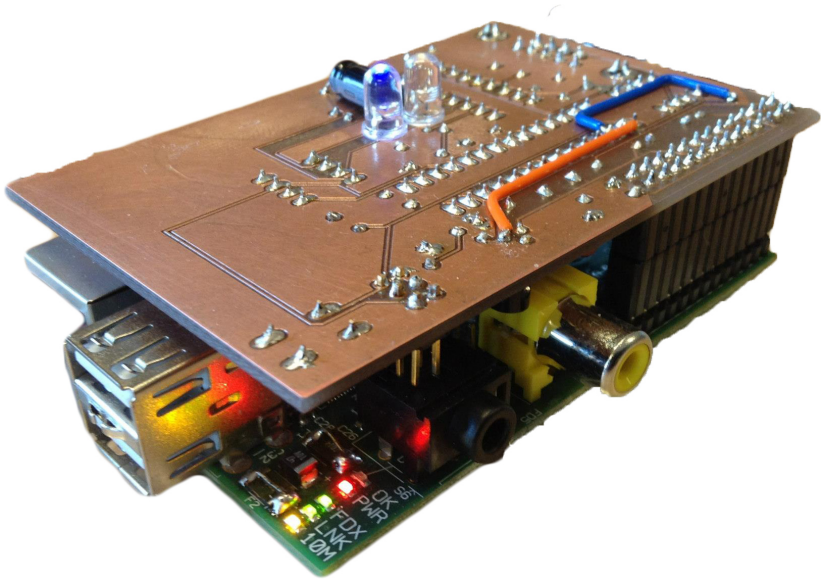

Figure 2.3: A picture of the completed embedded system, the CAN-bus interpreter is connected to the Raspberry Pi over their respective RS-232 serial ports.

2.2.1 Communication Test

The RSU was powered up and started broadcasting simulated traffic frames. A Drive C2X receiver was configured and all received wireless frames were saved to a binary file that was later inspected in Wireshark[4] using ITS-G5 dissectors[5]. The acquired frames could successfully be interpreted by the Wireshark dissectors, which meant that the RSU was generating valid GN, BTP and CAM frames with correct format and that the IEEE 802.11p modem was compatible with Drive C2X equipment.

2.2.2 Verification Test

During this test a setup with 3 main components was used; The RSU, a Drive C2X receiver and a Drive C2X Volvo car with an ITS-G5 implementation.

The RSU was installed and configured next to a road and the Drive C2X receiver was also installed and configured in the same spot. The Volvo car was

[4]Wireshark is a free and open-source packet analyzer.
[5]The ITS-G5 dissectors were fetched from AMB Consulting.

```
Latitude: 57°44'2647.69"N (577354698)
Longitude: 11°51'3102.12"E (118616989)
Speed: 10.44 m/s | 37.58 km/h (1044)
Heading: 5.4° (54)
```

(a)

```
Latitude: 57°44'2647.97"N (577355470)
Longitude: 11°51'3102.42"E (118617823)
Speed: 10.00 m/s | 36.00 km/h (1000)
Heading: 240.0° (2400)
```

(b)

Figure 2.4: Frame received from the RSU (A) and frame received from a Drive C2X Volvo car (B).

driven on the road next to the RSU a few times. The external Drive C2X receiver was capturing frames during this time.

Once the test was completed the captured frames were analyzed and compared side by side in Wireshark. An example of logged frames can be seen in Fig. 2.4. The logged frames were almost identical with the only deviation being the car's heading, as the heading reported by the RSU was in relation to the direction of the radar while the heading reported by the Drive C2X car was in relation to the North.

The radar bearing was roughly measured with a smartphone, and after compensating for the radar alignment the heading of the car was calculated to 230°, which is close to the reported heading of 240°, and within an acceptable error margin for a smartphone.

2.3 Accuracy Tests

Functional tests were performed on the RSU as mentioned above, but other aspects also needed to be tested. One of those was the accuracy of the reported time in conjunction with the accuracy of the coordinates in the GN/CAM frames down to centimetre level. Accuracy measurements were performed with the help of a state of the art GPS positioning device [33].

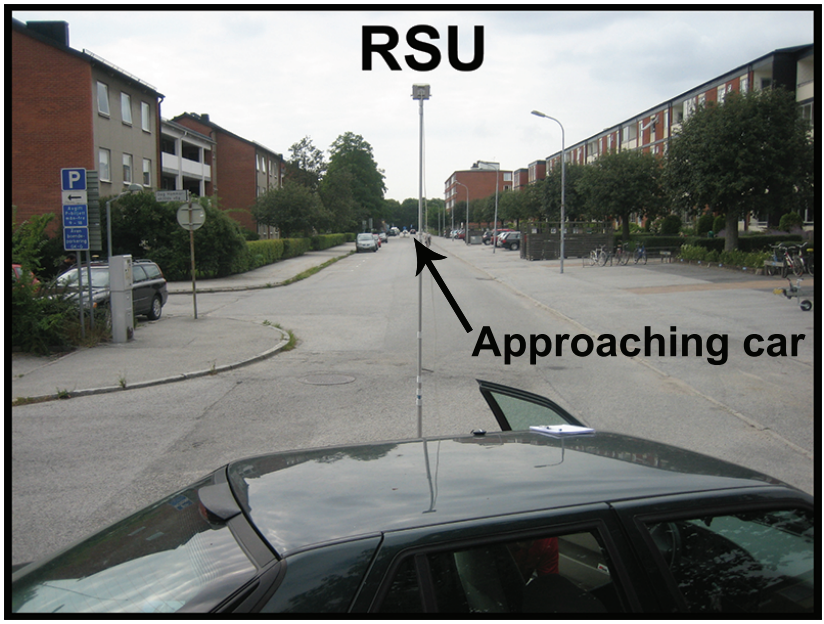

Figure 2.5: The RSU pointing towards the street.

2.3.1 Objectives

GeoNetworking and CAM frames contain a timestamp as well as the WGS84[6] geographic coordinates of a vehicle [3, 31]. It is very important that the reported timestamp is actually the correct timestamp when the vehicle was at the reported coordinate, because the accuracy of the position estimate depends on the accuracy of the time estimate. Delays might be introduced as a result of processing time that various algorithms utilize. Therefore, it is important to measure and report these delays and their impact on the accuracy of the position estimate.

2.3.2 Methodology

The measurement setup consisted of the RSU on a 5 m tripod, see Fig. 2.5, a high precision GPS receiver that reports coordinates with errors in the centimetre level range [33] mounted on a Volvo V70 car, see Fig. 2.6. A 350 m

[6]WGS84: World Geodetic System 1984, last revised in 2004 according to the National Geospatial-Intelligence Agency.

Figure 2.6: High accuracy GPS with an external antenna mounted on the top of the car.

straight patch of road selected as measurement route, see Fig. 2.7.

The car drove 22 times down the street towards the RSU while logging its coordinates and timestamps with the high precision GPS receiver. At the same time the RSU was detecting the car and also logging its coordinates and timestamps.

GPS time was used on both systems. A GPS receiver was temporarily fitted on the RSU for time synchronization. According to [34] GPS time is typically accurate within 40 ns, which is more than enough since the maximum logging resolution of the RSU is 1 ms.

2.3.3 Results

Time Errors

The first measurement was used as a calibration run. The goal with this measurement was to find possible errors in the time domain.

The RSU was using UTC time, since its network time protocol (NTP) daemon was compensating for leap seconds [35]. However, the GPS receiver was

Figure 2.7: The long straight part of Dag Hammarskjölds street in Lund, Sweden. The RSU was placed at point A pointing towards point B. Images: © 2013 Cnes/Spot Image, DigitalGlobe, Lantmäteriet/Metria. Map data: © 2013 Google.

using pure GPS time and therefore the extra leap seconds were compensated for the RSU. According to [36] the offset between GPS time and coordinated universal time (UTC) was 16 s as of the time of the measurements [37].

Also a millisecond level fine-tuning was done numerically on the time offset. The offset that minimized the distance error was selected.

Spatial Errors

The RSU can detect both distance to a vehicle (x-coordinate) and sidewise displacement of a vehicle (y-coordinate). Thus both directions and their errors were studied separately.

In order to find possible errors in the spatial domain all measurements were compensated for the time offset. The distance from the RSU to the car was compensated for the value that minimized the mean x-error, and the sidewise movement of the car was compensated for the position of the GPS device on the car.

In Fig. 2.8 a measurement sample can be seen. The difference in distance between the RSU and GPS data is the spatial error which can be seen in Fig. 2.9. However, what is more interesting to analyze is the error of all the measurements as a function of the distance from the RSU to the car as seen

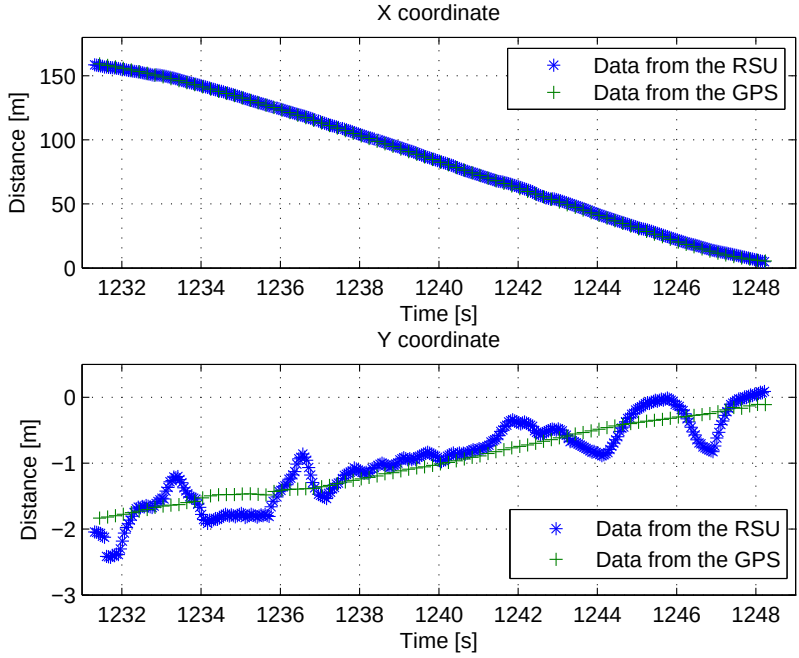

Figure 2.8: Positions reported during one of the 22 sample runs. The upper graph displays data for the distance from the RSU to the vehicle (x) and the lower graph displays data for the sidewise movement of the vehicle (y).

in Fig. 2.10. The root mean square error (RMSE) can be read as a measure of accuracy. For x; $RMSE_x = 248\,\text{cm}$ and for y; $RMSE_y = 38\,\text{cm}$.

When the car is within 28 m from the RSU, a deterministic behavior can be observed, as the car is going out of the main beam of the radar, as seen in section A of the upper graph of Fig. 2.10. A least squares model that describes this behavior can be found, reversed and added to the data in order to eliminate the error.

Vehicle Reference Point

It is also of interest to investigate whether the reference point of the RSU on the car is changing as the car is approaching the RSU. A slope different from zero on the least squares approximation in Fig. 2.10 would indicate that. As it can be seen the slope is near 0 both for the x and y directions. Therefore it is

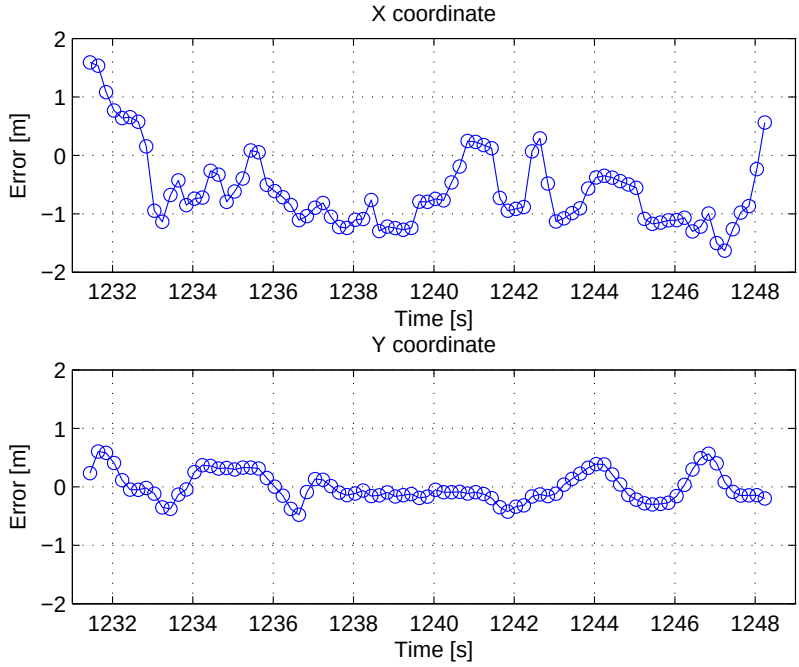

Figure 2.9: The error between RSU and GPS data from the same measurement as in Fig. 2.8, as a function of time.

indicated that the reference point of the RSU on the car is fairly static.

Weather Implications

Tests in various weather conditions, such as rain, snow and fog have not been performed. However, the system's detection performance is not expected to change significantly in bad weather conditions. According to the radar manufacturer [29], the radar *works in adverse conditions, almost unaffected by weather, and independent of sunlight, in a wide temperature interval* (−40 to +85 °C).

2.4 Smoothing and Path Prediction

As seen in the previous section, the RSU data is not error-free. Also, there are parts of measurements where the RSU cannot see the vehicle and it does not

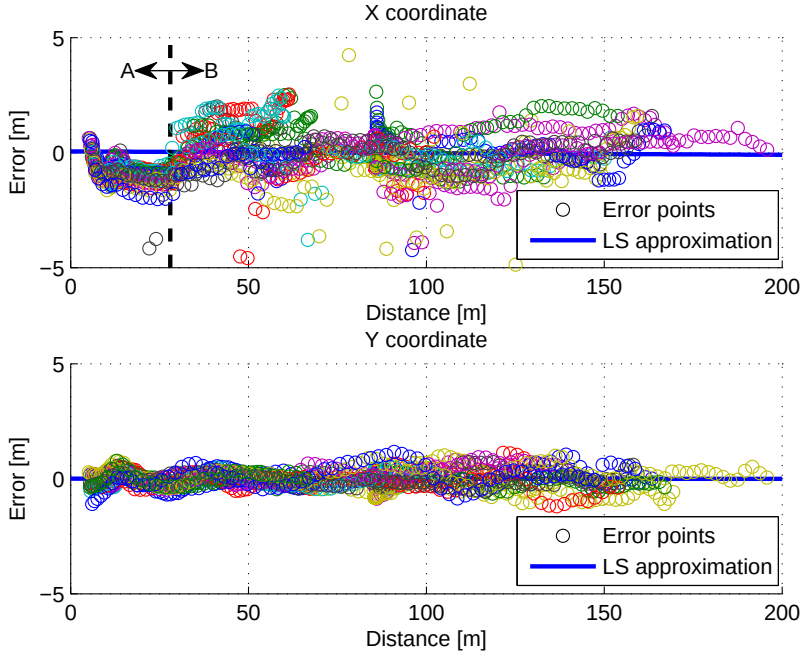

Figure 2.10: Scatter plot displaying the error as a function of distance from the RSU to the car for all measurements. For the x-coordinate a deterministic behavior can be seen near the radar in section A, which can be compensated for by an appropriate model. The least squares (LS) approximation of the upper part of the figure is based on data from section B. The root mean square (RMS) error for x is $RMSE_x = 248\,\text{cm}$ and for y is $RMSE_y = 38\,\text{cm}$.

report any data during that time. This can occur due to a shadowing effect or other disturbances.

In order to tackle those problems a Kalman filter has been introduced for the RSU data. A Kalman filter can produce a statistically optimal path estimate for some given noisy path observations given that the process model, process noise and measurement noise are known or can be estimated [38].

2.4.1 Dynamic Model

To describe the vehicle dynamics a constant velocity model (CV) [39, p. 338] has been used, as depicted below:

$$x_k = Ax_{k-1} + Bu_{k-1} + w_{k-1} \tag{2.1}$$
$$z_k = Hx_k + \nu_k, \tag{2.2}$$

where $x_k = [p_k \; v_k]^T$ is the state of the system, u_k is an optional control input, w_k is the process noise, z_k is the measurement, ν_k is the measurement noise and

$$A = \begin{bmatrix} 1 & \Delta t \\ 0 & 1 \end{bmatrix}, B = 0 \tag{2.3}$$
$$H = \begin{bmatrix} 1 & 0 \\ 0 & 1 \end{bmatrix} = I, \tag{2.4}$$

where Δt is the time between each measurement observation. Moreover, the process noise w_k and measurement noise ν_k are assumed to be normally distributed with mean $\mu = 0$ and covariance $\sigma_w^2 = Q$ and $\sigma_\nu^2 = R$ [40]. H is the identity matrix since there are measurements for both components of the state (position p_k and velocity v_k), and it is assumed that these measurements are independent.

2.4.2 Implementation

The Kalman filter implementation utilizes a recursive algorithm which consists of a time update, where the next state of the system is "predicted", and a measurement update, where the earlier prediction is "corrected". During the time update the following operations are performed:

$$\hat{x}_k^- = A\hat{x}_{k-1} \tag{2.5}$$
$$P_k^- = AP_{k-1}A^T + Q. \tag{2.6}$$

Also when there is a measurement observation at a certain time slot a measurement update is being performed with the following operations:

$$K_k = P_k^-(P_k^- + R)^{-1} \tag{2.7}$$
$$\hat{x}_k = \hat{x}_k^- + K_k(z_k - \hat{x}_k^-) \tag{2.8}$$
$$P_k = (I - K_k)P_k^-. \tag{2.9}$$

If a measurement observation is missing then the same operations are being performed but with Kalman gain set to zero:

$$K_k = 0 \tag{2.10}$$

$$\hat{x}_k = \hat{x}_k^- \tag{2.11}$$

$$P_k = P_k^-. \tag{2.12}$$

Here $\hat{x}_k^-$ and P_k^- are a priori (before measurement update) and $\hat{x}_k$ and P_k are a posteriori (after measurement update) state estimate and error covariance respectively. K_k is the Kalman gain. B and H are not seen in the equations above since $B = 0$ and $H = I$.

2.4.3 Parameter Estimation

The process noise covariance Q, measurement noise covariance R, initial error covariance P_0 and initial state vector $\hat{x}_0 = [\hat{p}_0 \ \hat{v}_0]^T$ are Kalman filter parameters that have to be estimated.

The process noise is often unknown and that complicates the estimation of the filter parameters. However, since the GPS data is much more accurate than the RSU data, it is assumed that the GPS data is error-free in order to get an acceptable filter parameter estimation. Also, as [40] states; *often times superior filter performance (statistically speaking) can be obtained by tuning the filter parameters Q and R.*

Q and R

The process noise covariance Q was calculated from the distribution of the GPS data noise and tuned in a way that minimizes the root mean square (RMS) measurement error:

$$Q_x = 10^{-3} \begin{bmatrix} 5.4212442813 & 0 \\ 0 & 8.1657541509 \end{bmatrix} \tag{2.13}$$

$$Q_y = 10^{-5} \begin{bmatrix} 7.0235962884 & 0 \\ 0 & 0.0130178705 \end{bmatrix}. \tag{2.14}$$

The measurement noise covariance R was similarly calculated by looking at the distribution of the error between the GPS and RSU data:

$$R_x = \begin{bmatrix} 2.4824824996 & 0 \\ 0 & 6.3782090266 \end{bmatrix} \tag{2.15}$$

$$R_y = 10^{-1} \begin{bmatrix} 1.4246746491 & 0 \\ 0 & 0.1792773482 \end{bmatrix}. \tag{2.16}$$

Both distributions were assumed to be Gaussian.

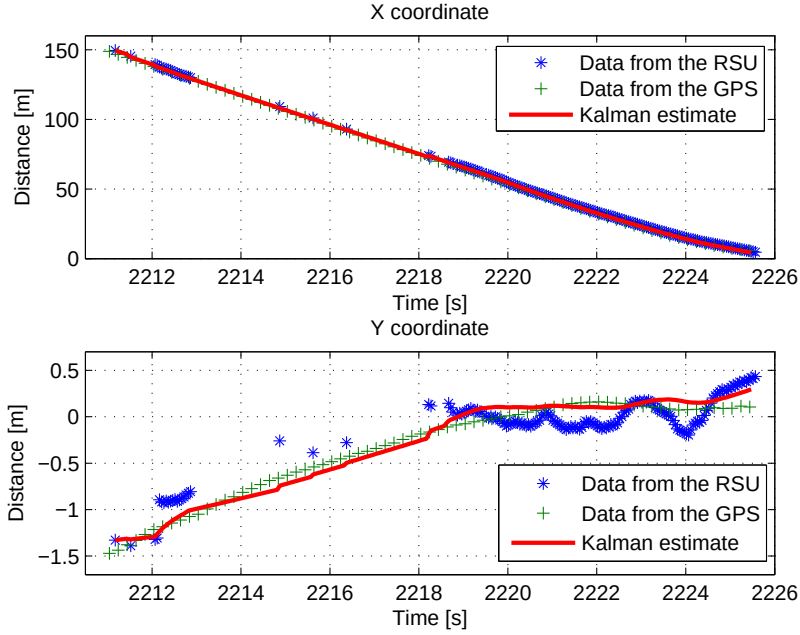

Figure 2.11: Positions reported during a bad run. The upper graph displays data for the distance from the RSU to the vehicle (x) and the lower graph displays data for the sidewise movement of the vehicle (y). It can be seen that the Kalman filter predicts and smoothens the path very well.

Initial Error Covariance P_0

The initial error covariance P_0 was set equal to the process noise covariance Q and tuned by a factor that minimizes the root mean square measurement error (RMSE):

$$P_0^x = \begin{bmatrix} 50 & 0 \\ 0 & 6000 \end{bmatrix} Q_x \tag{2.17}$$

$$P_0^y = \begin{bmatrix} 200 & 0 \\ 0 & 4000 \end{bmatrix} Q_y. \tag{2.18}$$

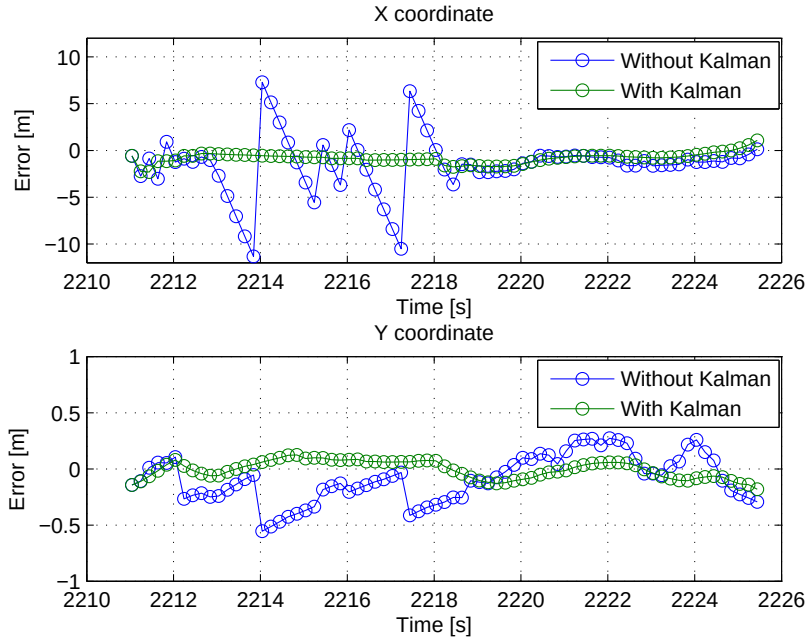

Figure 2.12: The error between RSU and GPS data from the same measurement as in Fig. 2.11, with and without Kalman filtering, as a function of time. It can be seen that the Kalman filter minimizes the error.

Initial State Vector $\hat{x}_0$

The initial state vector contains two components; the initial position $\hat{p}_0$ and the initial velocity $\hat{v}_0$. The initial position was set equal to the first measurement observation $\hat{p}_0 = z_0$ and the initial velocity was set equal to the mean velocity for each coordinate; $\hat{v}_0^x = -10.37\,\mathrm{m/s}$ and $\hat{v}_0^y = 0.06\,\mathrm{m/s}$.

2.4.4 Results

The aim with Kalman filtering was to smoothen and predict the path for gaps in the RSU data. As it can be seen in Fig. 2.11, 2.12 and 2.13 the goal has been reached.

The RMS measurement error for the x-coordinate has decreased from $RMSE_x = 248\,\mathrm{cm}$ to $RMSE_x = 146\,\mathrm{cm}$. The RMS measurement error for the y-coordinate has remained the same at $RMSE_y = 38\,\mathrm{cm}$. However, for most

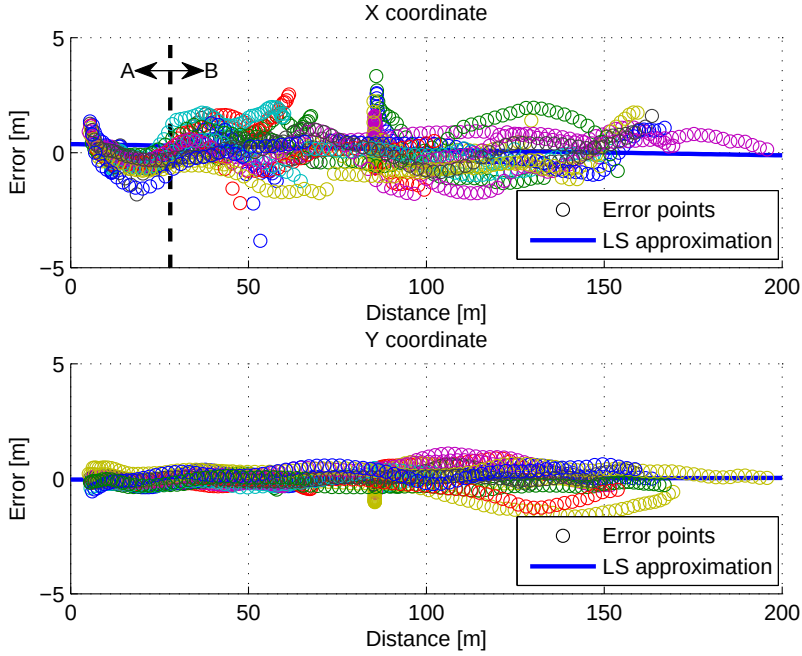

Figure 2.13: The same figure as Fig. 2.10. However, the error displayed here is after Kalman filtering has been applied on the data from the RSU. It can be seen that many outliers have been eliminated and the deterministic behavior in section A seems more predictable. The root mean square error (RSME) for x is $RMSE_x = 146\,\text{cm}$ and for y is $RMSE_y = 38\,\text{cm}$.

of the measurements, as the one depicted in Fig. 2.11 and 2.12, the error has decreased while it has increased only for few measurements which bring the RMSE up.

Chapter 3

Truck as an Obstacle

Vehicle-to-vehicle (V2V) communication is extremely beneficial in the situations where the visual line-of-sight (LOS) is obstructed by buildings or other taller vehicles. In an obstructed LOS (OLOS) situation scattering from the nearby objects, e.g., traffic signs, trucks and bridges, enables signal reception. Due to scattering and absence of a strong LOS component, which carries most of the power when available, the root mean square (RMS) values of delay and Doppler spreads tend to be very high and the power is spread out in both the time and frequency domains [41]. Thus, building reliable transceivers that can handle such a dynamic and lossy channel, is one of the biggest challenges in V2V communications.

Also, wireless channels in OLOS highway and urban scenarios provide severe challenges for the receiver according to previous studies [18, 42–48]. Inconveniently, those scenarios correlate largely with the use cases with the smallest margin for packet errors due to the high speeds and, often, heavy traffic density. A number of important vehicle-to-vehicle (V2V) scenarios involve multiple vehicles traveling in a convoy formation, including platooning, in which vehicles exchange acceleration and braking information wirelessly to maintain narrow following distances to save fuel and minimize shock waves through traffic. Non-adjacent vehicles driving in a convoy formation (or even adjacent vehicles with line-of-sight blocked by semi-trailers) impose OLOS links dependent on other propagation mechanisms. This scenario is relevant even for other use cases, such as hazardous location notification messages including slow-vehicle warnings or emergency brake light warnings. Two passenger cars with a truck blocking the line-of-sight between them is both a realistic and suitable scenario for building and testing an analytical model.

3.1 Related Work

Channel models have been developed and parametrized for vehicular communications based on the two-ray ground reflection model and simple path-loss models, mostly for LOS situations [49]. The effect of vehicles as physical obstructions is often disregarded in the models. There are a few studies, which investigate this impact based on theoretical considerations as well as on measurements.

Meireles *et al.* in [42] aim to clarify the validity of this simplification, that the effect of vehicles as physical obstructions is often disregarded, in parking lot, highway, suburban and urban canyon environments. Detailed measurements in a parking lot were also reported in [46]. The conclusion is drawn that a single vehicular obstacle can cause an additional loss between 10-20 dB in the received signal strength.

Boban *et al.* in [43], investigated further the impact of vehicles as obstacles and presented a model verified by experimental measurements that satisfies accurate positioning, realistic mobility patterns, realistic propagation characteristics and manageable complexity.

A measurement-based shadow fading model based on real traffic measurements performed in urban and highway scenarios is then developed by Abbas *et al.* in [50], for V2V network simulations. An additional attenuation of about 10 dB, a value similar to the previous studies, was experienced on average due to obstructing vehicles.

The importance of the vehicle type in the shadowing distribution is also highlighted by Segata *et al.* in [45].

Obstruction by a truck is investigated in terms of RF link range and packet error rate (PER) by Gallagher and Akatsuka in [51]. It has been found that the PER increases in average by 52.7 % for an average distance of 144.2 m when the transmitted power decreases from 29 dBm to 20 dBm. All of these studies considered single antenna systems, with roof mounted antennas only.

He *et al.* [46] investigate the scenario of a car-bus-car convoy. The bus is acting either as a blocking object or a relay. They present measurement results and model the propagation channel. The influence of the bus and the separation distance between the cars is analyzed on the path loss, shadowing, small-scale fading, delay spread, and cross correlation. It was found that the main effect of the bus is an additional attenuation of 15 to 20 dB and an increase in the root mean square (RMS) delay spread by roughly 100 ns. The distance dependence of the path loss is analyzed and a stochastic model is developed for it.

Mahler *et al.* [52] investigate the 6 GHz propagation channel between oncoming vehicles with five different types of obstructing vehicles in a poor scattering environment. Different antenna positions and their advantages are in-

vestigated in one straight and one curved road scenario. Similarly to this thesis and [18], rural roads in open fields were used for measurements, as they are very good examples of poor scattering environments. In the straight road scenario, where most of the received power is can be attributed to diffraction, at a distance of 300 m, the channel gain was shown to be around -110 dB.

To the author's best knowledge, besides [51] which investigates mainly packet error rate, there is no study available investigating the impact of OLOS on time-frequency selective properties as well as on multi-antenna systems with diversity arrangement, i.e., when antennas are mounted at different locations on a car. This thesis deals with these aspects, where a truck is used as an obstacle in a controlled way in a highly dynamic environment. Also, a valid model for the power contribution due to diffraction around a truck has not yet been presented. Diffraction is the main contributor of power in obstructed line-of-sight scenarios in rural environments that are characterized by poor scattering [52]. It is important to investigate whether communication through diffraction is still possible in these scenarios.

3.2 Contributions

The contribution of this thesis is parametrization of the path loss, shadow fading, delay-Doppler spreads, and the additional loss as a function of distance between TX and RX, that a system will exhibit when a truck acts an obstacle in rural and highways scenarios. It has been seen that sudden shadowing from a truck can cause an additional mean loss of 9-13 dB depending on the antenna location and selected scenario. In-depth characterization of the OLOS situation, with a truck as an obstacle, is very important as it may occur often in real traffic.

A model for the power contribution of signal components diffracting around a truck is also proposed. Unlike the stochastic model for the path loss developed in [46], which is based on empirical measurement data, the model described in this thesis is purely analytical and theoretical. It requires rough knowledge of the geometry of the propagation scenario, including vehicle sizes and distances. A rural propagation environment is assumed where scattering is poor and the only received power is due to diffraction around the truck. Any additional scattering due to dissimilar environments will only increase the channel gain.

3.3 Measurements

Measurements were conducted in the surroundings of the city of Lund, Sweden. Two cars acted as transmitter (TX) and receiver (RX) and one truck as an

Figure 3.1: The two cars at TX/RX and the truck as obstacle used in the measurements. The total truck length was 9.8 m with a container width of 2.6 m and height of 4.0 m from the ground.

obstacle. GPS coordinates and videos were recorded from each vehicle. The participating vehicles can be seen in Fig. 3.1. Two major measurement scenarios were considered: Rural and Highway. For each scenario there were both line-of-sight (LOS) and obstructed line-of-sight (OLOS)[1] short term (ST) and long term (LT) measurements.

3.3.1 Measurement Setup

Multiple-input single-output (MISO) measurements were performed by collecting channel transfer functions $H(f,t)$ for each TX–RX antenna pair based on the switched-array principle, using the RUSK LUND channel sounder [53]. The TX car incorporated 6 antennas while the RX car incorporated a single roof antenna. On the TX four antenna elements were mounted on the roof and two additional antennas were mounted inside the vehicle, at the front and rear

[1] OLOS is defined as the situation were the truck was purposely placed in-between the RX and TX during measurements.

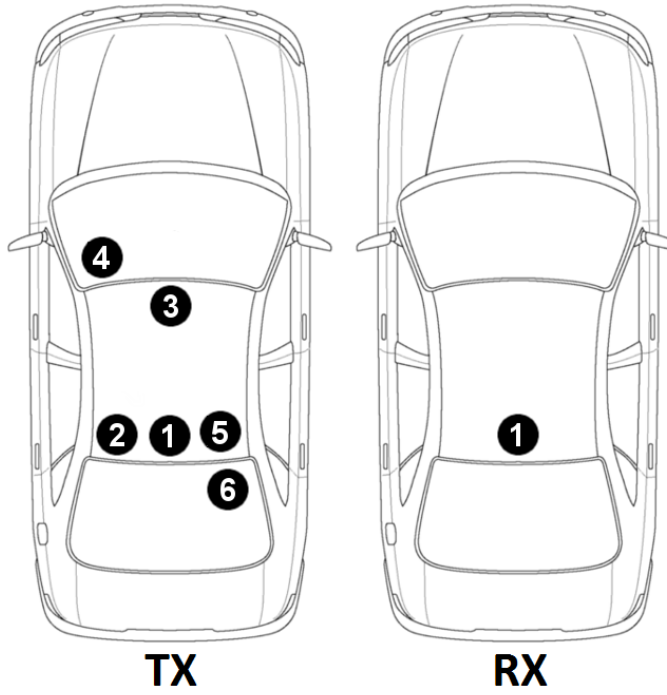

Figure 3.2: Antennas placement on the TX and RX cars. **TX:** Antennas 1, 2, 3 and 5 were omni-directional shark-fin antennas mounted on the roof of the car. Antennas 4 and 6 were omni-directional antennas mounted inside of the front and rear windshields respectively. **RX:** A single omni-directional antenna was mounted on the roof of the car.

windshields, in order to analyze the possibility of having hidden antennas inside the car. The antennas were mounted as seen in Fig. 3.2. The most important measurement parameters are shown in Table 3.1.

All the antenna elements were omni-directional in the azimuthal plane, but the antenna pattern after mounting them is certainly not. This is important when investigating which antenna positions are the most appealing for different traffic scenarios. Abbas *et al.* in [54] have shown that the best reception performance can be obtained by combining antennas with complementary properties, e.g., a roof and a bumper antenna. In this thesis bumper antennas are not investigated but a comparable diversity gain is expected from the windshield antennas since they experience similar shadowing properties to some degree.

While many measurements were performed, only a few were selected for the

Table 3.1: Measurement Parameters

Parameter	**Value**
Center frequency, f_c	5.75 GHz
Bandwidth, B	200 MHz
Test signal length, $\tau_{\max}$	3.2 μs
Time between snapshots, t_{rep}	268.8 μs (ST), 93 ms (LT)
Number of samples in time, N_t	65000 (ST), 120000 (LT)
Number of samples in frequency, N_f	641
Recording time, t_{rec}	18 s (ST), 563 s (LT)
Number of TX antennas	6
Number of RX antennas	1
TX antenna height	145 cm (roof), 135 cm (windshield)
RX antenna height	160 cm (roof)

analysis in this thesis. Measurements with a high dynamic range were used, which was determined by visual inspection of power delay profiles and the video recordings from within the vehicles.

3.3.2 Scenario Description

Two scenarios were considered during these measurements; Rural and Highway. There were 16 measurements taken in total.

Rural Scenario

The rural scenario took place on Odarslövsvägen (55°44'07.7"N, 13°15'46.3"E). The average speed was 19.4 m/s (70 km/h). It consisted solely of short term measurements. All measurements were conducted in a convoy formation where the TX was in the front, the RX was in the back and the truck was in the middle whenever present. Rural measurements were conducted as reference measurements in an environment where few or no scatterers are present. Odarslövsvägen is characterized by low traffic and wide open fields. Houses are few and distant, 100–200 m from the road. Such a poor scattering environment is expected to provide clear and controlled measurements with the only multipath components arising either from the line-of-sight or the diffraction around the truck.

Highway Scenario

The highway scenario took place on E22 in both the North and South directions outwards from Lund. The average speed was 25 m/s (90 km/h). It consisted of 7 short term and 2 long term measurements. Of those, 4 were LOS and 5 were OLOS measurements. E22 is a European highway characterized as a road with low to heavy traffic, guard rails on its outer edges, separating concrete blocks, bridges and other structures. These measurements are expected to characterize a rich scattering environment.

3.4 Channel Characterization

The subsequent analysis will include only three TX antennas 1, 4 and 6. There are three main reasons that these three antennas are preferred over others. First, the antennas 1, 2, and 3 on the back of the roof are all highly correlated, which is concluded by looking at the channel gains, however antenna 1 is the best antenna from a design point of view and it also gave the best results in most of the cases among the three located at the back of the roof. Most modern vehicles already have a shark fin antenna installed there for other wireless applications (GPS, LTE/WCDMA/GSM). Second, antennas 3 and 4 exhibit similar behavior, where as reception at antenna 4 is the best among the two due to multipath components that arrive from the front of the car. Finally, antenna 6 is the one that complements antenna 4 and in turn provides a significant diversity gain compared to each other. Therefore, antenna 4 and 6 together can be used as a multi-antenna solution with complementary arrangement.

All losses from cables and channel sounder equipment were measured prior to these measurements. Therefore all gain values that are presented here are from TX antenna switch to RX antenna. Similar cables were used between switch and antenna connectors, thus any changes in the gain are only due to the effect of the channel.

3.4.1 Path Loss

Since the measurements were conducted in a controlled environment, it was easy to separate LOS and OLOS situations. However, sometimes other vehicles interrupted LOS momentarily. By inspection of video recordings from inside the vehicles, those interruptions were considered as OLOS during the analysis.

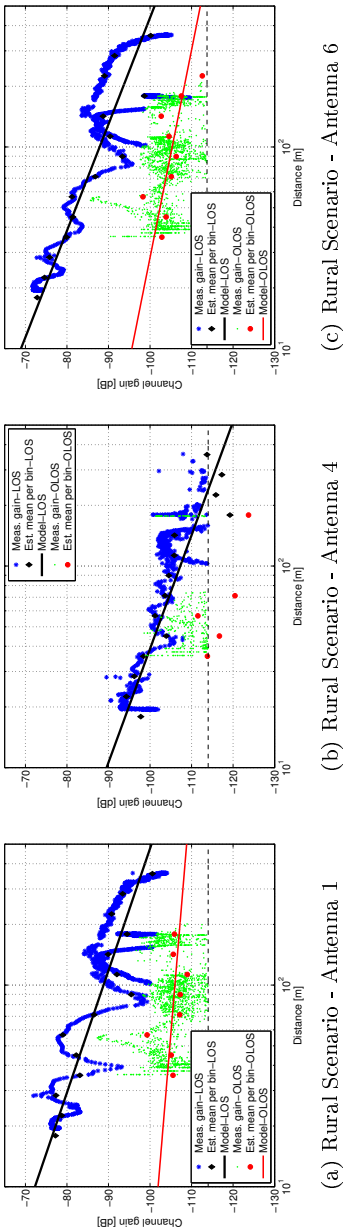

(a) Rural Scenario - Antenna 1

(b) Rural Scenario - Antenna 4

(c) Rural Scenario - Antenna 6

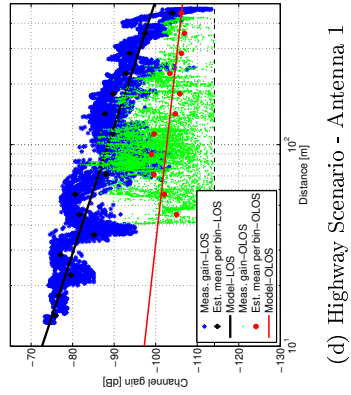

(d) Highway Scenario - Antenna 1

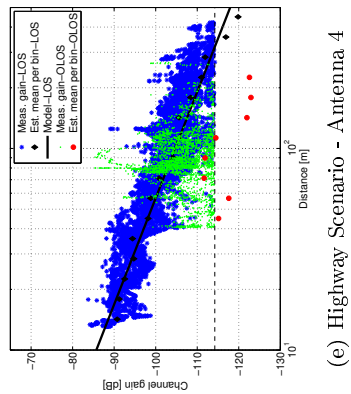

(e) Highway Scenario - Antenna 4

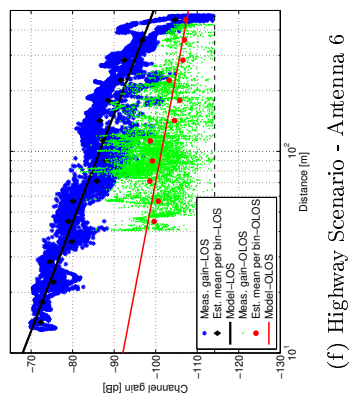

(f) Highway Scenario - Antenna 6

Figure 3.3: Channel gain for each antenna for the rural and highway scenarios and the best path-loss fit in a least-squares sense [55]. The estimated bin-mean values are plotted for each dataset according to [56].

The channel gain is plotted in Fig. 3.3 as a function of distance for both LOS and OLOS. The path loss is modeled using log-distance power law given as

$$P(d) \quad = \quad P_{d_0} - 10nlog_{10}\left(\frac{d}{d_0}\right) + X_\sigma\,, \tag{3.1}$$

where $P(d)$ is the received power at a given distance d. The path-loss exponent n and channel gain P_{d_0} at 10 m reference distance, which give deterministic value of path loss, were estimated by fitting equation (3.1) to both the LOS and OLOS datasets using linear regression in the least square sense. X_σ is the large-scale fading on top of the deterministic path loss, which is zero mean Gaussian random variable with some time correlation. The standard deviation (σ) of the large-scale fading is estimated by subtracting the distance dependent path loss from the channel gain data and looking at the distribution properties of the remaining Gaussian dataset. As evident from Fig. 3.3, the channel gain due to poor channel conditions momentarily falls below noise threshold at certain distances. Since the exact count of the data points below noise threshold is known, the standard deviation can easily be estimated from incomplete data via expectation maximization (EM) by using a broadly applicable algorithm presented in [56, 57] that iteratively computes maximum likelihood estimates (MLE). The estimated parameters can be found in Table 3.3. Path loss was not modeled for the OLOS case of antenna 4 since most of the data is below the noise floor and such an estimation would not be accurate. However the estimated bin-mean values are still presented as a reference as seen in Fig. 3.3.

The expected critical distance breakpoint due to two-ray ground reflection model where the path loss exponent is equal to 4 according to theory could not be clearly observed here. Thus it was not taken into consideration as one single slope seems to fit the data well in both the LOS and OLOS cases. However, the power received adjacent to the truck in the OLOS case is quite low in comparison with the power received at a small distance from the truck. That causes the path-loss exponent n to be quite small for the OLOS cases.

Another interesting fact is that the highway scenario exhibits a higher gain for the OLOS case in comparison to the rural scenario. That is due to a rich scattering environment with guard rails, separating concrete blocks, bridges and other structures, with multipath components arising from more sources than solely diffraction around the truck. This behavior can be observed in Fig. 3.3 as well as in Table 3.2.

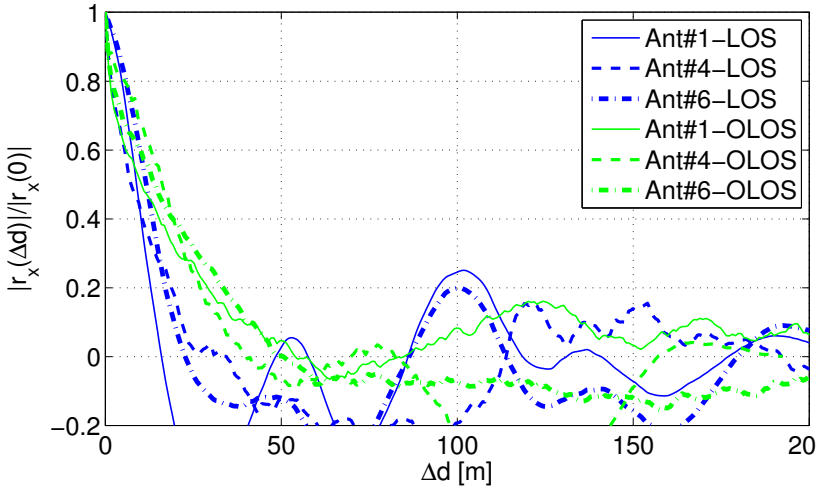

(a) Rural scenario.

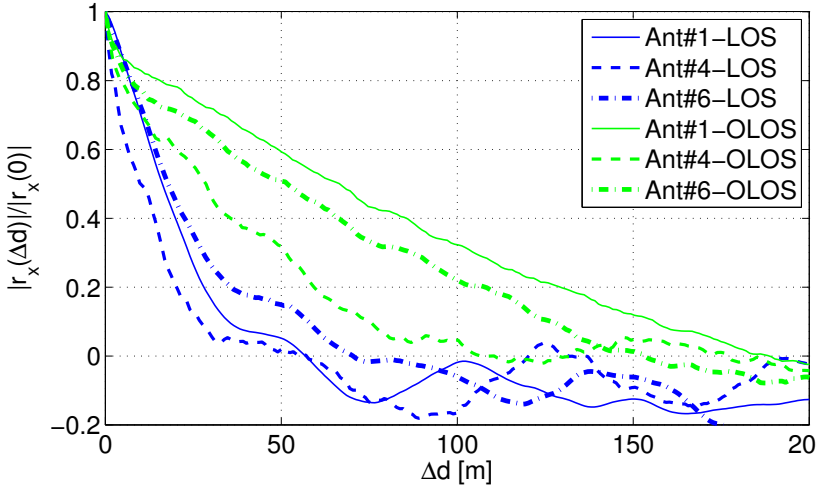

(b) Highway scenario.

Figure 3.4: Spatial correlation of large-scale fading in rural and highway scenarios.

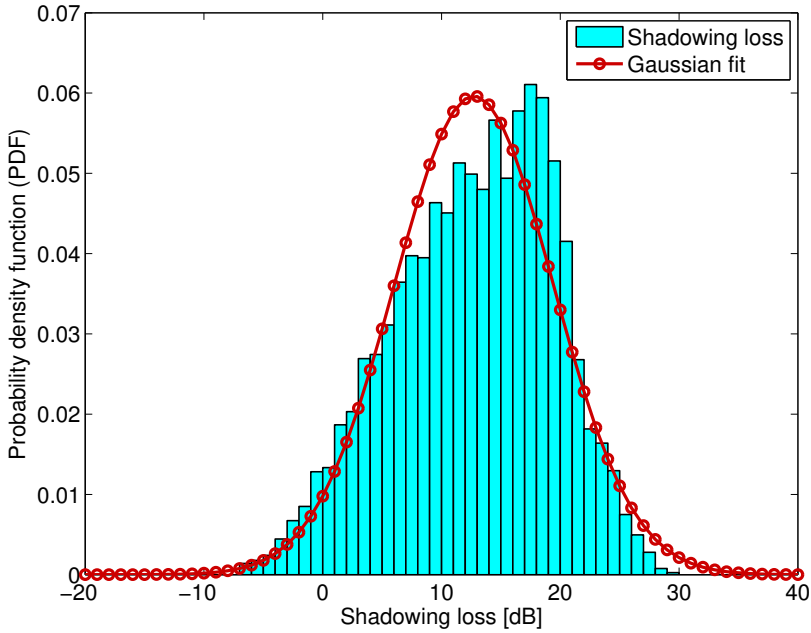

Figure 3.5: Shadowing loss due to the truck for antenna 1 in the highway scenario.

3.4.2 Large-Scale Fading

The large-scale fading was modeled as a Gaussian random variable with mean equal to zero and standard deviation σ. The results can be found in Table 3.3. Since the distance dependent mean path loss is already subtracted from the data, the large-scale fading can assumed to be a stationary time series whose joint distribution does not change over time. The spatial correlation of the large-scale fading, which is also an interesting parameter to investigate, can then be obtained by an auto-correlation of this time series as

$$r_x(\Delta d) = E\{X_\sigma(d)X_\sigma(d+\Delta d)\}\,. \tag{3.2}$$

The spatial correlation of the shadow fading is shown in Fig. 3.4. From the plots it can be seen that the spatial correlation in the OLOS situation is higher than that in the LOS situation. It is mainly due to the difference in underlying propagation mechanisms, i.e., the measured path loss in the LOS, follows the two-ray ground reflection model that results in fluctuations in the power at regular distance intervals for the distances below breakpoint distance. However,

Table 3.2: Shadowing Loss, $L_{\text{shadow}} \sim \mathcal{N}(\mu_{\text{loss}}, \sigma^2_{\text{loss}})$

	Rural			**Highway**		
Antenna	A1	A4	A6	A1	A4	A6
μ_{loss} [dB]	11.9	10.0	8.9	12.7	10.7	10.8
σ_{loss} [dB]	5.2	6.2	5.0	6.7	6.0	6.0

that is not the case in OLOS in which the measured path loss is more random with larger variations than that in LOS and it does not follow the two-ray ground reflection model either. Moreover, the spatial correlation in the highway scenario is higher than that in the rural scenario because of differences in the scattering environment, e.g., on the highway, in contrary to the rural scenario, there are several scattering objects such as road signs and overhead bridges that provide strong specular reflections and in turn better received power as long as they are visible to both TX and RX.

The shadow fading correlation can be modeled by a well known analytical model by Gudmundson [58], which is a simple negative exponential function

$$r_x(\Delta d) = e^{-|\Delta d|/d_c}\,, \tag{3.3}$$

where Δd is equally spaced distance vector and d_c is the decorrelation distance at which the value of the auto-correlation function is equal to e^{-1}. The d_c distance for both scenarios is specified in Table 3.3.

3.4.3 Shadowing Loss

The loss due to shadowing from the truck, which is a function of distance between the TX and RX, was calculated by subtracting the mean path loss in LOS from the OLOS dataset. As an example, the resulting dataset for one of the antennas can be seen in Fig. 3.5. It was found that it can be described as a Gaussian random variable with a mean μ_{loss} and a standard deviation σ_{loss}. Those values are reported in Table 3.2 for each TX–RX antenna pair.

3.4.4 RMS Delay and Doppler Spreads

The RMS delay and Doppler spreads are measures of the channel dispersion in the time and frequency domains respectively. By looking at Fig. 3.6 one can conclude that both the RMS delay and Doppler spreads increase for the OLOS case. Moreover, one can see that antenna 4 behaves differently in comparison to antennas 1 and 6. That is due to the fact that it is shadowed by the body

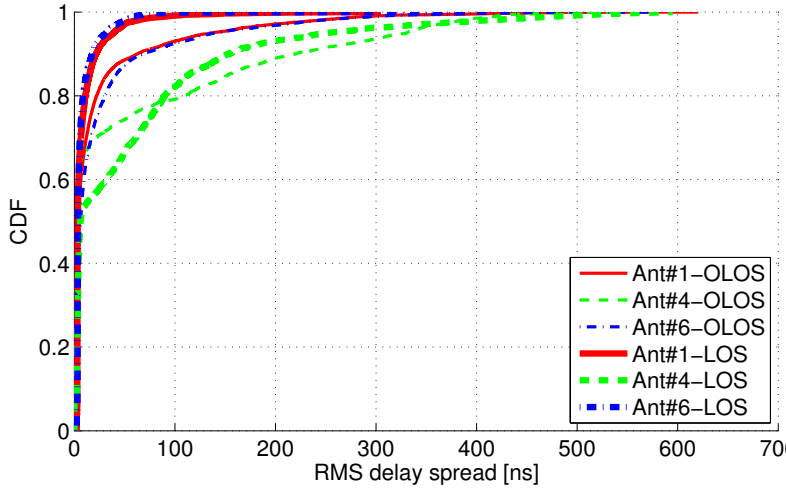

(a) RMS Delay Spread.

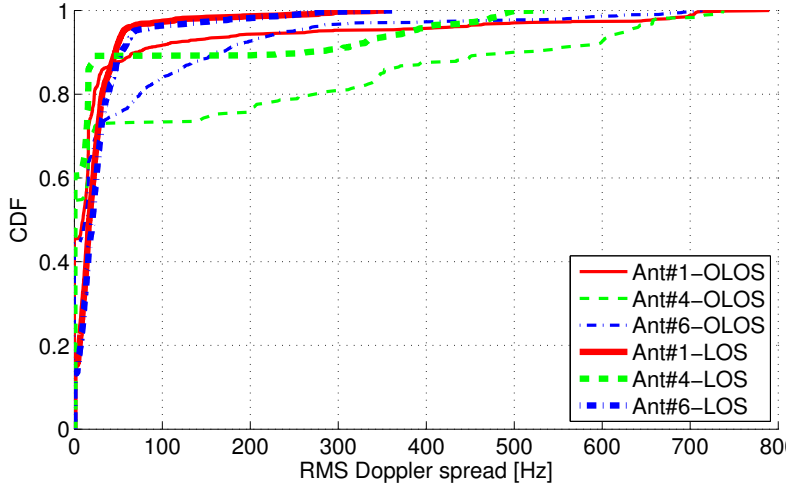

(b) RMS Doppler Spread.

Figure 3.6: RMS Delay and Doppler spreads for LOS and OLOS for all antenna pairs.

of the car itself and no dominant multipath component is arriving at antenna 4.

Table 3.3: Analyzed Parameters. Values for P_{d_0} and n are not included for antenna 4 due to the fact that most of the samples were below the noise floor, thus they were not modeled as seen in Fig. 3.3.

		LOS			**OLOS**		
	Antenna	A1	A4	A6	A1	A4	A6
Rural	P_{d_0} [dB]	-72.3	-89.6	-68.9	-101.9	——	-95.6
	n	1.65	1.77	1.89	0.41	——	0.97
	σ [dB]	3.9	8.4	4.9	5.4	13.9	5.1
	d_c [m]	10.1	11.3	13.6	16.8	20.2	21.0
	$\mu_{\tau_{\text{rms}}}$ [ns]	8.0	8.0	8.0	23.1	23.1	23.1
	$max_{\tau_{\text{rms}}}$ [ns]	331.5	702.0	97.5	651.7	604.6	645.6
	$\mu_{\nu_{\text{rms}}}$ [Hz]	13.8	47.2	13.2	12.1	1.3	8.1
	$max_{\nu_{\text{rms}}}$ [Hz]	375.7	816.0	167.7	281.1	14.1	261.6
Highway	P_{d_0} [dB]	-72.6	-85.7	-68.0	-97.2	——	-92.1
	n	1.60	1.90	1.86	0.54	——	0.93
	σ [dB]	4.4	7.9	4.0	7.3	17.0	6.5
	d_c [m]	20.5	14.3	24.0	89.0	40.9	69.5
	$\mu_{\tau_{\text{rms}}}$ [ns]	9.9	9.9	9.9	24.7	24.7	24.7
	$max_{\tau_{\text{rms}}}$ [ns]	304.6	595.2	388.6	620.3	545.8	581.0
	$\mu_{\nu_{\text{rms}}}$ [Hz]	24.8	45.2	28.9	44.2	117.1	52.9
	$max_{\nu_{\text{rms}}}$ [Hz]	353.7	534.3	361.1	789.9	737.4	712.6

3.5 Diffraction Model

Six multi-path components (MPCs) are considered in the model as shown in Fig. 3.7.

- MPC1: Above the truck (A-D-E)
- MPC2: TX ground reflection (B-C-D-E)
- MPC3: RX ground reflection (A-D-F-G)
- MPC4: TX & RX ground reflection (B-C-D-F-G)
- MPC5: Right side of the truck (H-J-L)

- MPC6: Left side of the truck (I-K-M)

Reflections under the truck are not considered as their contributions were assumed to be negligible during modeling due to a large number of reflections.

The main power contributions in the model come from MPC1. However, it is important to also consider other MPCs, some to a lesser and some to a higher extent, as ground reflections and different propagation distances alter the phase component of each MPC and lead to destructive interference at certain distances between the TX and the RX.

3.5.1 Propagation Mechanisms

Each MPC is characterized by an electrical field E_{MPC}. This section describes how propagation, reflection and diffraction interact with the transmitted electrical field. For the representation of an electrical field, a phasor, also known as complex amplitude, is used [13].

Propagation

For transmission between TX and RX, the free-space path loss (FSPL) equation, also known as Friis' law [13], was utilized. The amplitude and phase of the propagating electrical field is given by equation 3.4. Since the amplitude of the propagating field is being tracked, and not power, the square root of Friis' is considered:

$$E_{\text{fspl}}(d) = \frac{\lambda}{4\pi d} \cdot e^{\frac{j2\pi d}{\lambda}}. \tag{3.4}$$

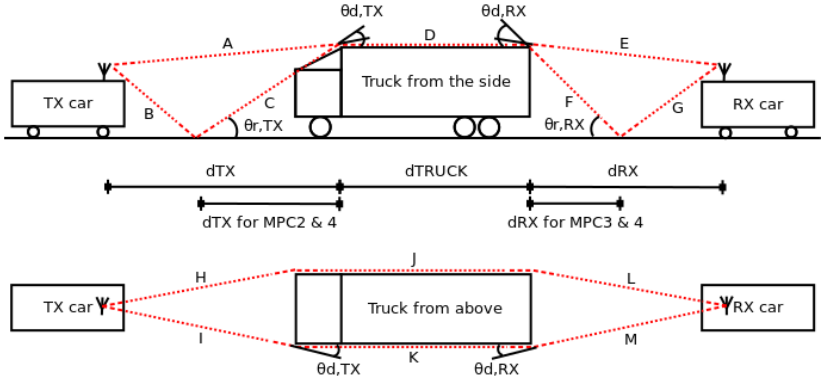

Figure 3.7: The multi-path components considered in the model.

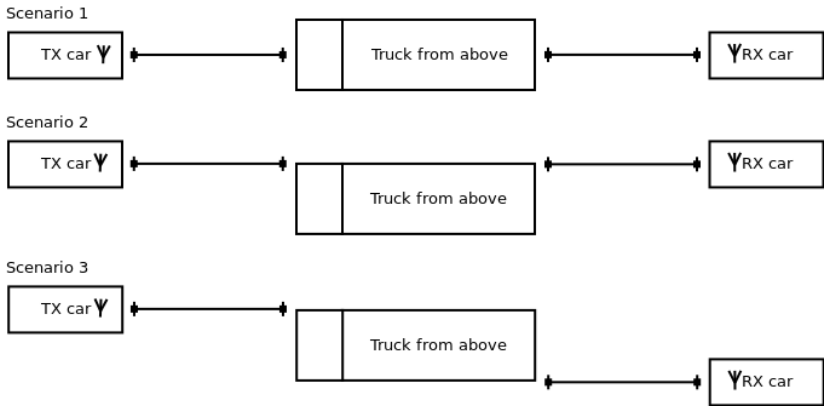

Figure 3.8: Scenario 1: Both cars are aligned with the center line of the truck. Scenario 2: Both cars are aligned with the same side of the truck. Scenario 3: One car is aligned with one side of the truck and the other car is aligned with the other side of the truck.

Here λ is the wavelength and d is the propagation distance between TX and RX for the MPC.

Reflection

The reflection coefficient Γ [59] was calculated for each MPC ground reflection. The reflection coefficient is a complex factor that scales the amplitude and shifts the phase of the electrical field that reflects on the ground. Γ is given by (3.5) and (3.6) assuming that the TX and RX antennas are vertically polarized.

$$X(\theta_\mathrm{r}) = \frac{\sqrt{\varepsilon - \cos^2\theta_\mathrm{r}}}{\varepsilon} \text{ for vertical polarization,} \tag{3.5}$$

$$\Gamma(\theta_\mathrm{r}) = \frac{\sin\theta_\mathrm{r} - X(\theta_\mathrm{r})}{\sin\theta_\mathrm{r} + X(\theta_\mathrm{r})}. \tag{3.6}$$

Here θ_r is the reflection angle between the MPC and the ground plane and ε is the relative effective complex permitivity of the ground. Assuming that the electrical properties of the ground reflection can be approximated by a single fixed effective permitivity value, it is modelled as $\varepsilon = 5 - 0.2j$ based on results from [60]. The model results do not differ significantly when ε is changed, thus it can be concluded that a small change in the permitivity value ε is not significant at small reflection angles θ_r.

Diffraction

Based on the assumption that both TX and RX are in the far field, the Epstein-Petersen method [61] with two screens was used in the calculation of the diffraction coefficient for each MPC diffraction. The diffraction coefficient $\tilde{F}(\nu_{\mathrm{F}})$ is given by

$$\tilde{F}(\nu_{\mathrm{F}}) = \frac{1}{2} - \frac{e^{j\pi/4}}{\sqrt{2}} F(\nu_{\mathrm{F}}), \tag{3.7}$$

where $F(\nu_{\mathrm{F}})$ is the Fresnel integral which is given by

$$F(\nu_{\mathrm{F}}) = \int_0^{\nu_{\mathrm{F}}} e^{-j\pi\frac{t^2}{2}} dt, \tag{3.8}$$

where ν_{F} is the Fresnel parameter. The Fresnel parameter is different for each screen and is given by

$$\nu_{\mathrm{F}_1} = \theta_{\mathrm{d,TX}} \sqrt{\frac{2 \cdot d_{\mathrm{TX}} \cdot d_{\mathrm{TRUCK}}}{\lambda(d_{\mathrm{TX}} + d_{\mathrm{TRUCK}})}} \tag{3.9}$$

$$\nu_{\mathrm{F}_2} = \theta_{\mathrm{d,RX}} \sqrt{\frac{2 \cdot d_{\mathrm{TRUCK}} \cdot d_{\mathrm{RX}}}{\lambda(d_{\mathrm{TRUCK}} + d_{\mathrm{RX}})}}, \tag{3.10}$$

where θ_{d} is the diffraction angle. The diffraction angle depends on the height of the TX/RX antenna or the height of the ground (0 for MPCs with ground reflection) on each respective side, the height of the two screens, and the distance between the TX/RX and each respective screen. It can be easily derived using Euclidean geometry. d_{TX} is either the distance from the first screen to the TX or the distance from the first screen to the ground reflection on the TX side, depending on whether the MPC of interest reflects on the ground or not. d_{RX} is described similarly but on the RX side. d_{TRUCK} is the length of the truck. See Fig. 3.7 for an illustration of the distances.

3.5.2 Implementation

The model channel gain, denoted G_{dB}, is given by as the power of the total electric field E_{total} in dB:

$$E_{\mathrm{total}} = E_{\mathrm{MPC1}} + E_{\mathrm{MPC2}} + E_{\mathrm{MPC3}} + E_{\mathrm{MPC4}} + E_{\mathrm{MPC5}} + E_{\mathrm{MPC6}}\,, \tag{3.11}$$

$$G_{\mathrm{dB}} = 20\log_{10}|E_{\mathrm{total}}|\,. \tag{3.12}$$

Above the Truck

For the multi-path component that propagates above the truck, MPC1, the electric field is defined as the transmitted field scaled by the diffraction coefficients for the first and second screens and is given by

$$E_{\mathrm{MPC1}} = \tilde{F}(\nu_{\mathrm{F}_{1,\mathrm{MPC1}}}) \cdot \tilde{F}(\nu_{\mathrm{F}_{2,\mathrm{MPC1}}}) \cdot E_{\mathrm{fspl,MPC1}}\,. \tag{3.13}$$

One Ground Reflection

The electric field of the multi-path components that have exactly one ground reflection, i.e. MPC2 and MPC3, is defined as the transmitted field scaled by the reflection coefficient on each side and the diffraction coefficients for the first and second screens. The fields are given by

$$E_{\mathrm{MPC2}} = \Gamma(\theta_{\mathrm{r,TX}}) \cdot \tilde{F}(\nu_{\mathrm{F}_{1,\mathrm{MPC2}}}) \cdot \tilde{F}(\nu_{\mathrm{F}_{2,\mathrm{MPC2}}}) \cdot E_{\mathrm{fspl,MPC2}}\,, \tag{3.14}$$

$$E_{\mathrm{MPC3}} = \Gamma(\theta_{\mathrm{r,RX}}) \cdot \tilde{F}(\nu_{\mathrm{F}_{1,\mathrm{MPC3}}}) \cdot \tilde{F}(\nu_{\mathrm{F}_{2,\mathrm{MPC3}}}) \cdot E_{\mathrm{fspl,MPC3}}\,. \tag{3.15}$$

Two Ground Reflections

The multi-path component that undergoes two ground reflections, MPC4, is defined similarly to MPC2 and MPC3. However, in this case the transmitted electric field needs to be scaled by the reflection coefficient on both sides of the truck. The field is given by

$$\begin{aligned} E_{\mathrm{MPC4}} &= \Gamma(\theta_{\mathrm{r,TX}}) \cdot \Gamma(\theta_{\mathrm{r,RX}}) \\ &\cdot \tilde{F}(\nu_{\mathrm{F}_{1,\mathrm{MPC4}}}) \cdot \tilde{F}(\nu_{\mathrm{F}_{2,\mathrm{MPC4}}}) \cdot E_{\mathrm{fspl,MPC4}}\,. \end{aligned} \tag{3.16}$$

Around the Truck

The multi-path components propagating around each side of the truck, MPC5 and MPC6, are defined similarly to MPC1. However, in this case the height of the screens is the width of the truck and the height of the TX/RX antennas depends on the lateral position of the cars in relation to the truck.

Three scenarios, scenario 1–3 as seen in Fig. 3.8, have been defined to illustrate the outcome of the model and to be able to compare with measured channel data in the *Verification* section.

The electric fields on each side depend on the scenario and are given by

$$E_{\mathrm{MPC5}} = \tilde{F}(\nu_{\mathrm{F}_{1,\mathrm{MPC5}}}) \cdot \tilde{F}(\nu_{\mathrm{F}_{2,\mathrm{MPC5}}}) \cdot E_{\mathrm{fspl,MPC5}}, \tag{3.17}$$

$$E_{\mathrm{MPC6}} = \tilde{F}(\nu_{\mathrm{F}_{1,\mathrm{MPC6}}}) \cdot \tilde{F}(\nu_{\mathrm{F}_{2,\mathrm{MPC6}}}) \cdot E_{\mathrm{fspl,MPC6}}. \tag{3.18}$$

3.5.3 Verification

The proposed model has been evaluated for a number of different realizations. Realizations of scenarios 1–3 can be seen in Fig. 3.9. The only difference between those realizations is the lateral position of the TX and RX. In the same figure one can see the model maximum, minimum and mean as well as standard deviation of the dB values of 40000 realizations. Those realizations were derived by creating 200x200 channel realizations for all possible lateral positions of the TX and RX. By selecting this resolution the minimum lateral step of each car was $2.6\,\mathrm{m}/200 = 13\,\mathrm{mm}$ or ca $\lambda/4$ at $5.75\,\mathrm{GHz}$.

By comparing the measured log-normal mean with the model log-normal mean one can conclude that the model renders real life scenarios rather accurately, in spite of the model being purely theoretical. Also, one can not overlook the fact that the model maximum, out of all the 40000 realizations, accurately predicts the measured data maximum, where it even tracks the bumpy trends of the measured data.

Fig. 3.10 was rendered to give an intuition of the field in-front of the truck, for different positions of the RX car behind the truck. In-fact it doesn't matter which side of the truck that is being depicted in the figure, as long as it can be assumed that the channel is reciprocal. As expected one can see that the channel gain is much more favorable towards the sides of the truck. It is also noticeable that the channel gain is low near the truck while it increases going away from it only to decrease again as path loss comes through.

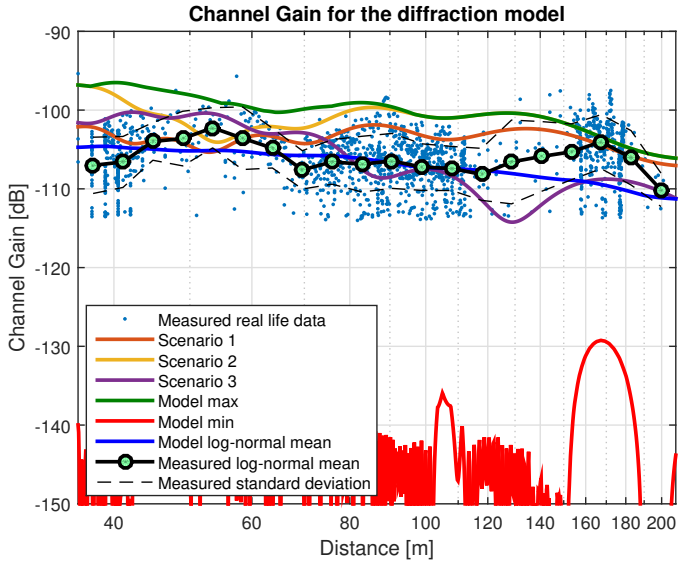

(a) The proposed model zoomed-in to measured channel data region.

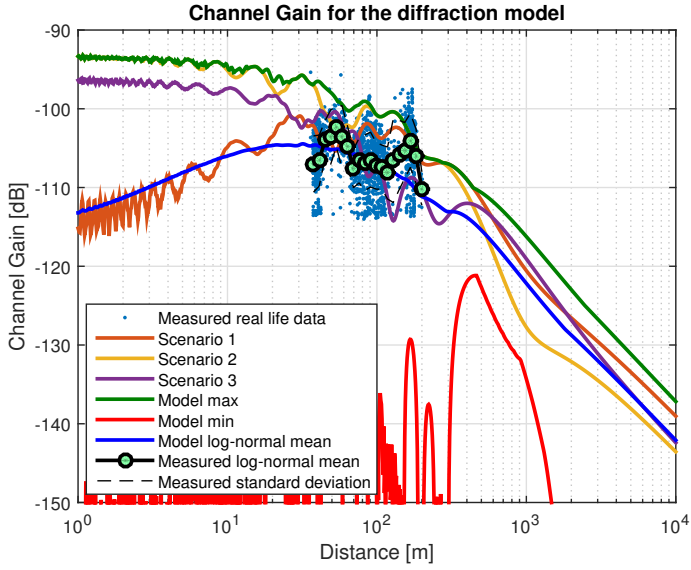

(b) The proposed model extrapolated outside of the measured channel data region. One can observe that the model log-normal mean and scenario 1 mostly coincide with each other and there is a low received power region adjacent to the truck up to ca 10 m.

Figure 3.9: Measured channel gain compared to different scenarios generated by the proposed model.

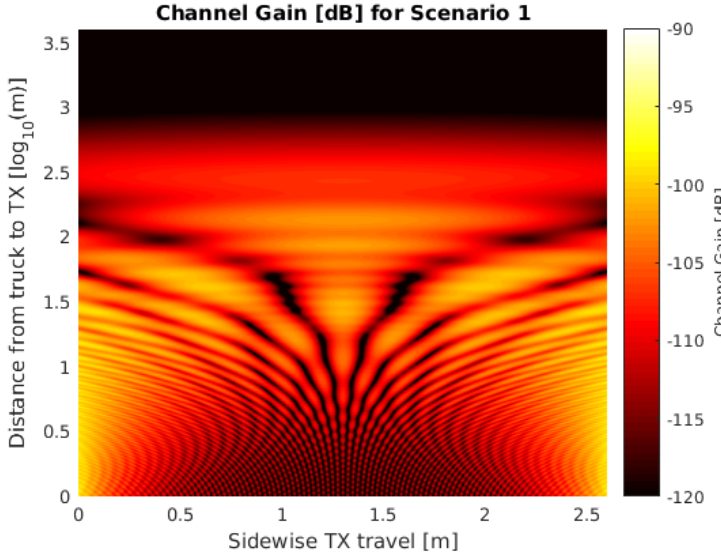

(a) Channel gain for the spatial field in front of the truck when the RX is right in the middle behind the truck. Scenario 1 is realized when the TX is right in the middle in front in the truck at 1.8 m sidewise travel.

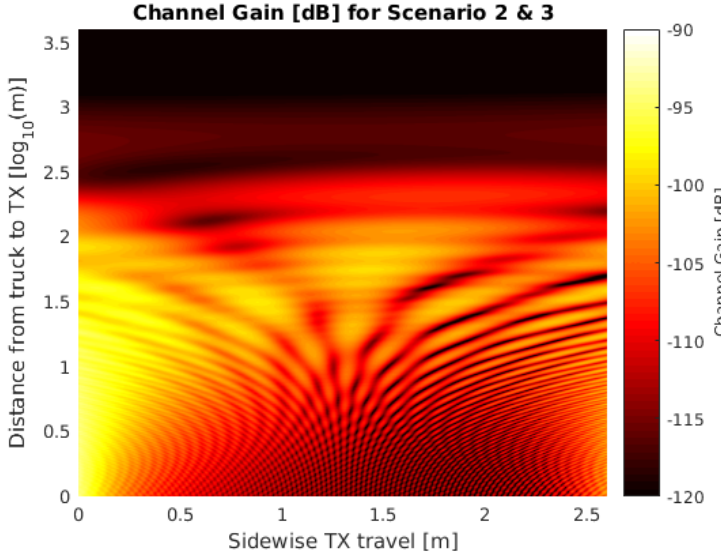

(b) Similar to Fig. 3.10(a) but for scenario 2 and 3. The RX in this case is all the way to the left behind the truck. Scenario 2 is realized when the TX is at 0 m sidewise travel and scenario 3 is realized when the TX is at 2.6 m (full width of the truck) sidewise travel.

Figure 3.10: The channel gain in-front of the truck for two different positions of the car behind the truck.

Chapter 4

Channel Emulation

A real-time wireless channel emulator for wireless vehicular communications based on a software defined radio (SDR) can enable quick on-bench evaluation of wireless transceivers while providing a high degree of reconfigurability. The SDR used in this thesis is an NI USRP-2943R [62] equipped with 2 Radio Frequency (RF) chains and an Xilinx Kintex-7 field programmable gate array (FPGA) programmable in LabVIEW, which allows real-time 2x2 MIMO or 1x1 full-duplex SISO channel emulation. This thesis describes a 1x1 SISO channel emulator as the standard IEEE 802.11p does not utilize MIMO technologies. A multiple antenna extension of the emulator is though straightforward. For vehicular transceiver characterization, a stress test that allows for a straightforward evaluation of modem capabilities is proposed. The stress test focuses on three important capabilities of vehicular modems; the ability to handle large Doppler spreads, the ability to handle short signal outages (e.g. due to ground reflections) and the ability to handle large delay spreads. This stress test is implemented and two different modem implementations are characterized using this methodology.

Earlier work on channel emulation has been done by a few companies. National Instruments has developed an example application for a real-time MIMO channel emulator based on a vector signal transceiver (VST) [63]. Nilsson *et al.* in [64] describe a multipath propagation simulator (MPS) that simulates the wireless channel using multiple antennas, long fiber-optic delay lines and phase shifters. A demo of another channel emulator based on SDR has been presented by M. Gurcan in [65]. Furthermore, Spirent [66] and Anite [67] also provide commercial solutions for channel emulation. However, to the authors best knowledge, such a platform based on SDR has not been previously openly developed and evaluated in the academic community.

4.1 Design & Implementation

4.1.1 Model

Assuming that the wireless channel for shorter time intervals can be seen as wide sense stationary, it can be modeled as a tapped delay line, where the coefficients multiplying the output from each tap vary with time [13]. The impulse response of the channel can be modeled as

$$h(t,\tau) = \sum_{i=1}^{N} c_i(t) \cdot \delta(\tau - \tau_i), \tag{4.1}$$

where N is the number of taps, $c_i(t)$ is the time-dependent complex coefficient and τ_i is the delay of the ith tap. For the stress test, a special case of this channel is applied: a two-tap channel where both taps have equal amplitudes but where the Doppler shift and delay of the second tap is varied while logging the packet error rate (PER). The complex coefficient for the second tap is given by

$$c_i(t) = \alpha \cdot e^{j2\pi f_{D_i} t}, \tag{4.2}$$

where α is the amplitude and f_{D_i} is the Doppler shift.

Two different IEEE 802.11p modem implementations have been evaluated by the channel emulator and the stress tests. Two modems, from now on denoted as modem group A, are early prototypes based on a modified IEEE 802.11a WiFi chipset, and therefore are not expected to perform optimally in a vehicular environment. The other two modems, from now on denoted as modem group B, are dedicated IEEE 802.11p modems and are expected to perform better. A two-tap delay line model, $N = 2$, was implemented on the FPGA of the SDR, where the first tap always remains at delay $\tau_1 = 0\,\text{ns}$ and Doppler shift $f_{D1} = 0\,\text{Hz}$. The second tap varies its delay in the range $\tau_2 \in \{100...3400\}\,\text{ns}$ (corresponding to $\{30...1020\}\,\text{m}$) in 34 steps and its Doppler shift in the range $f_{D2} \in \{0...2000\}\,\text{Hz}$ (corresponding to $\{0...366\}\,\text{km/h}$) in 41 steps. Additionally, the amplitude is set to $\alpha = 1$ for both taps, which generates a worst-case scenario. If the modems can manage such a scenario, they can manage weaker signals from the second tap as well, which serves as a reasonably good benchmark between different groups of modems. The ranges of the Doppler frequency shifts and delays were selected based on earlier studies and reasonable operation ranges in the parameter space. By moving the second tap to various points in the Doppler-delay domain, it is possible to log the packet error rate for each channel setting and characterize the modems' capabilities.

The choice of a two-ray channel with amplitude $\alpha_1 = \alpha_2$ should be motivated. Two-ray channels are observed when there is a single strong reflection. In vehicular environments such a reflection may arise from the ground, a strong reflection from a bridge or a sign. In the case of a ground reflection, the Doppler shift of the second ray is expected to be $f_{D2} \approx 0$ while the amplitude and delay are expected to be $\alpha_1 \approx \alpha_2$ and $\tau_1 \approx \tau_2$, respectively. In the case of a strong reflection, e.g. from a sign, the Doppler shift of the line-of-sight (LOS) component is expected to be $f_{D_1} \approx 0$ for vehicles driving in convoy. However, the Doppler shift of the reflected ray f_{D2} is expected to be proportional to twice the speed of the vehicle. Meanwhile, the amplitude and delay of both taps are expected to be $\alpha_1 \approx \alpha_2$ and $\tau_2 \geq \tau_1$, respectively. In case of a far reflection, the delay and amplitude are $\tau_2 \gg \tau_1$ and $\alpha_2 \ll \alpha_1$, respectively in general, but with $\alpha_2 \approx \alpha_1$, as a worst case scenario that may arise when the LOS is blocked.

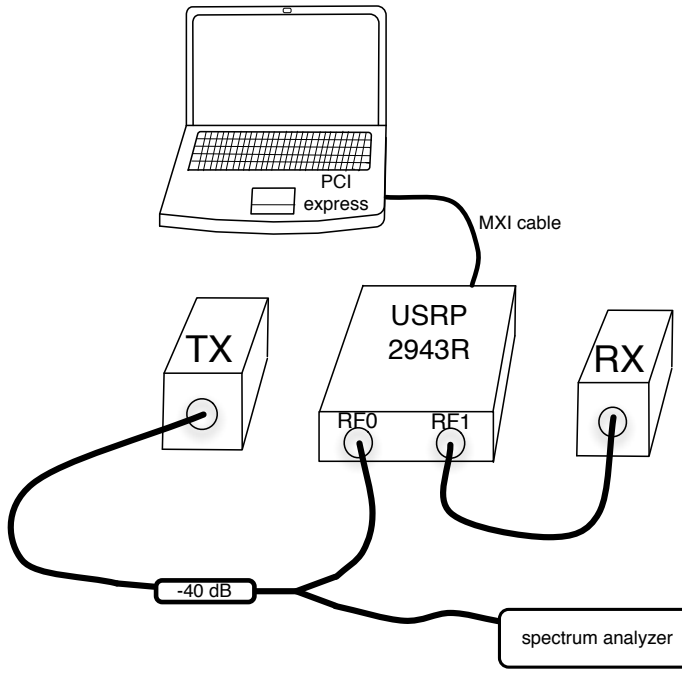

Figure 4.1: The overall system including a laptop running LabVIEW, two modems under test and an SDR. The spectrum analyzer is used for monitoring purposes.

All of these cases are covered using the approach in this thesis.

4.1.2 Overall System

The overall system consists of a laptop running LabVIEW, two modems and the SDR emulating the channel as shown in Fig. 4.1. A standard laptop with a PCI express card slot functions as the host computer, connecting to the SDR via an MXI cable. The host running LabVIEW is responsible for deploying FPGA bitfiles to the integrated FPGA and configures the RF-chains, i.e. sets active RF-chains, transmit power levels, received signal power reference levels, sampling rates, center frequencies and initializes active RF-chains. Furthermore, it is storing, post-processing and graphically displaying data from the SDR using target-to-host direct memory access (DMA) first-in first-out (FIFO) buffers.

The modems to be characterized are labeled as TX and RX, depending on if they act as transmitter or receiver. The TX modem is connected to one of the RF-chains, RF0, of the SDR with a 40 dB attenuator to protect the SDR. The signal is split to allow monitoring of the incoming signal using a spectrum analyzer. The received signal in the SDR is quantized to a 16-bit binary representation of in-phase (I) and quadrature (Q) components after the analog-to-digital converter (ADC) and downconversion, as the ADC makes use of oversampling. Thereafter, the received signal is fed through the FPGA of the channel emulator. After channel emulation in the FPGA, the digital signal is upconverted and fed to the digital-to-analog converter (DAC) to be transmitted through the other RF-chain, RF1, which is connected to the RX modem. The use of two separate RF-chains reduces leakage between receive and transmit signal tremendously, as the isolation between receiver and transmitter on the same RF-chain is only 30 dB. A picture of the complete system can be seen in Fig. 4.2.

4.1.3 Channel Emulation Core

Implementing a run-time configurable 2-tap delay line model on an FPGA-based SDR is achieved using a structure as shown in Fig. 4.3, where the input and output data are 32-bit complex values, consisting of 16-bit I and Q components, respectively.

To move along the delay domain, an at run-time configurable varying length shift-register is used. Each tap delays the input by 100 ns, and as the branch to extract data from the shift register moves along the taps, relative delays from $\tau_2 \in \{100...3400\}$ ns are achieved for the second tap whereas the first tap will not have any relative delay.

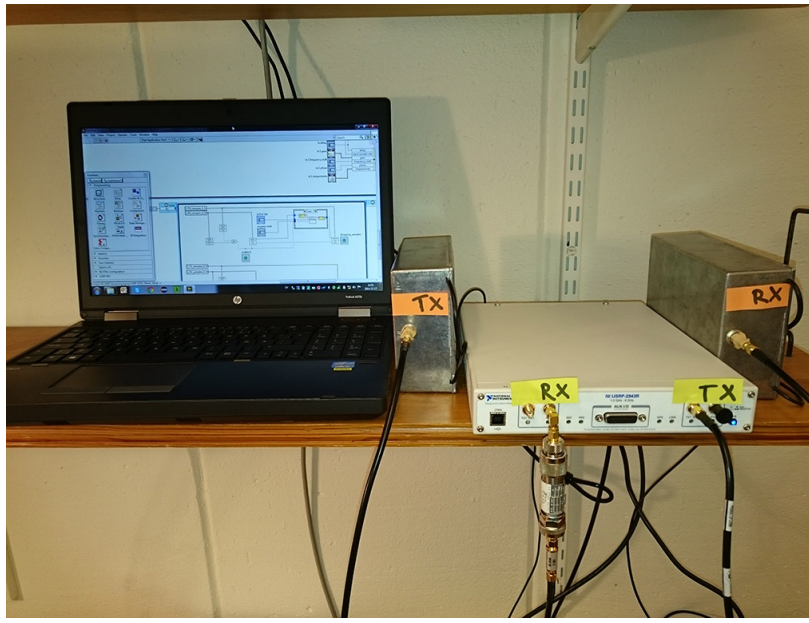

Figure 4.2: The complete system operating on the bench.

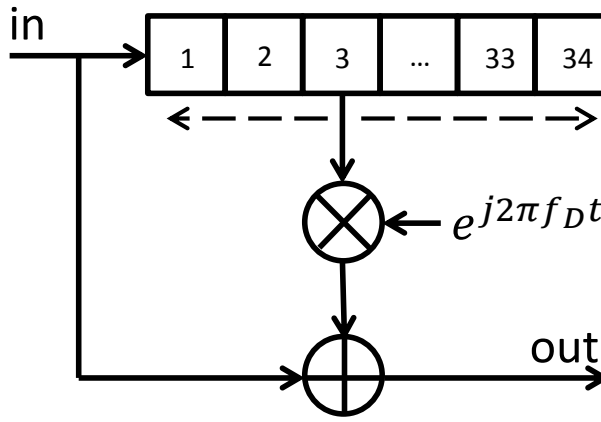

Figure 4.3: Hardware implementation of a run-time configurable 2-tapped delay line model using a parameterizable shift register.

Table 4.1: Test scenarios

Scenario nr	Modem group	Over-the-air packet size
1	Modem A	100 bytes
2	Modem A	500 bytes
3	Modem A	1500 bytes
4	Modem B	100 bytes
5	Modem B	500 bytes
6	Modem B	1500 bytes

Table 4.2: Measurement parameters

Parameter	Value
Link capacity	6 Mbit/s
Center frequency	5.9 GHz
Emulated channel bandwidth	10 MHz
Sampling rate	40 MS/s
Resolution in the delay domain	100 ns
Resolution in the Doppler domain	50 Hz
Number of transmitted packets per channel	600

Movement in the Doppler domain is achieved by varying $f_{D2} \in \{0...2000\}$ Hz in the complex exponential, equation (4.2), of the multiplier. Actual values to be used, are streamed from the host to the SDR using a host-to-target DMA FIFO during run-time. Both signals, the first tap and the delayed, Doppler-shifted second tap are combined using a complex adder, efficiently implementing equation (4.1).

4.2 Stress Test

The TX and RX modems to be characterized were connected as described previously. For both sets of modems, once the channel emulator started emulating the channel, the transmitter (TX) started transmitting packets with sequence numbers and dummy payload. On the receiver (RX) side, the sequence numbers were collected and the packet error rate was calculated based on the number of missing sequence numbers. Once the receiver monitored and stored the PER for a certain Doppler-delay combination, new channel parameters were loaded to the channel emulator and a new PER calculation was performed.

The test scenarios of the two modem implementations, as specified in Table 4.1, were evaluated in order to characterize the modems and examine the influence of different packet sizes on the packet error rate. In each scenario 200 packets per second were transmitted, resulting to a worst case utilization of

$$\frac{200\,\text{packets/s} \cdot 1500\,\text{bytes/packet} \cdot 8\,\text{bit/byte}}{6.0\,\text{Mbit/s}} = 40\,\%$$

of the link capacity, thus not congesting the link. Each channel configuration lasted 3 seconds. Therefore, 41 Doppler shifts $\cdot$ 34 delays $=$ 1394 possible Doppler-delay combinations were evaluated in $3\,\text{s} \cdot 1394\,\text{combinations} =$ 70 minutes for each scenario, which is a relatively fast evaluation time for on-bench stress tests. Further measurement parameters are given in Table 4.2.

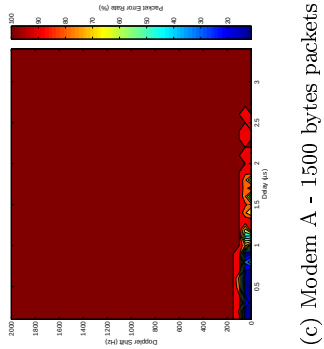

(a) Modem A - 100 bytes packets

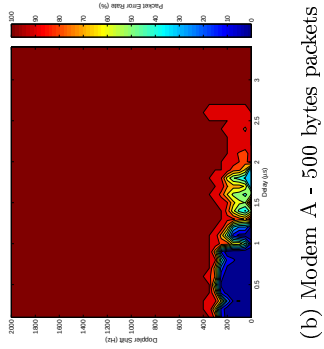

(b) Modem A - 500 bytes packets

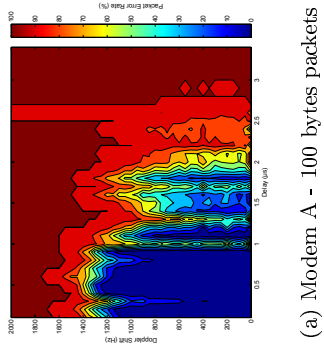

(c) Modem A - 1500 bytes packets

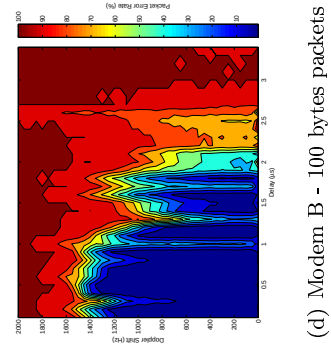

(d) Modem B - 100 bytes packets

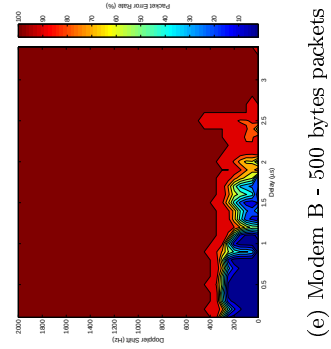

(e) Modem B - 500 bytes packets

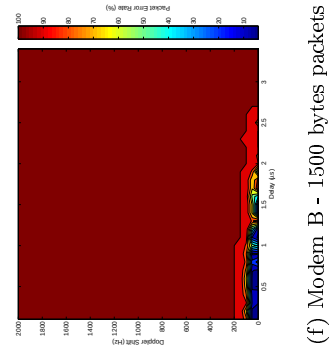

(f) Modem B - 1500 bytes packets

Figure 4.4: Packet error rate for early prototype (A) and dedicated (B) IEEE 802.11p modems and different packet sizes. The early prototype modems were based on a modified IEEE 802.11a WiFi chipset.

4.3 Performance

The modem performance after stress testing is shown in Fig. 4.4. Several observations can be made based on these results.

Firstly, the packet error rate increases with increased packet size which is quite intuitive since the channel estimates are based on the preambles in each packet; the larger the packets are the bigger time is required for transmission. However, increased packet size does not influence the packet error rate if the Doppler shift is $f_{D2} \approx 0\,\text{Hz}$, as expected.

Secondly, modem implementation B performs slightly better for increased Doppler shifts for delays above $1\,\mu\text{s}$. However, with increased packet size that improvement becomes insignificant and both implementations of modems perform similarly.

Thirdly, the packet error rate for both modem implementations increases dramatically in the proximity of 1.3–1.9μs which coincides with the length of the IEEE 802.11p OFDM cyclic prefix of $1.6\,\mu\text{s}$ [68] (which corresponds to 480 m propagation delay).

Overall, the performance of both groups of modems decreases significantly with increased packet size. Generally acceptable good performance with a PER $< 10\,\%$ is only achieved with small packet sizes.

Chapter 5

Conclusions and Future Work

5.1 Conclusions

This licentiate thesis presents, discusses, and shows results for several different research questions around obstructed and non line-of-sight scenarios in wireless vehicular communication.

In chapter 2 a road side unit (RSU) that implements the ITS-G5 standard has been described. It is able to emulate vehicle-to-everything (V2X) communications of non-intelligent vehicles within the sight of a radar, thus providing a better integration of ITS-G5 vehicles in the future. An embedded system succeeds on connecting a microwave radar and an IEEE 802.11p modem, providing an intelligent device in the middle that is powerful enough to perform all needed calculations. Functional tests have been performed in order to confirm the RSU's ability to communicate with other devices that implement the same standard and to verify the system's reported values such as coordinates and speed. Both tests have been successful. Accuracy tests have been performed and the system's accuracy shows promising results. The accuracy in x and y directions has been measured to 248 cm and 38 cm respectively when using raw RSU data. Kalman filtering has also been applied to the RSU data. As a result the reported positions from the RSU are smoother, continuous and more accurate. After filtering has been applied the RMS error in x and y directions has decreased to 146 cm and 38 cm, respectively.

With this technology, intelligent transportation will be realized earlier during the implementation phase, where just a small portion of vehicles on public roads will feature a cooperative communications system. It is also a long-term solution, since older vehicles will keep driving on public roads for a long time. By implementing the system in blind spots, intelligent vehicles will benefit from

extra active safety as they will be warned about surrounding vehicles.

Vehicular communications in rural and highway scenarios often experience power degradation due to the shadowing effect from other vehicles. Previous work has been done in this subject [42, 43, 45, 46, 50, 51]. However, to the author's best knowledge, the scenario of a truck as an obstacle in a controlled highly dynamic environment hasn't been investigated in-depth before. Chapter 3 considers this scenario. Additional losses of 12 and 13 dB have been found for the antenna with the best placement, from a channel and design point of view, in rural and highway scenarios respectively when shadowed by a truck, confirming previous results. Switched array 1x6 SIMO measurements were performed with the RUSK LUND channel sounder. The rural scenario took place in a poor scattering environment with wide open fields. The highway scenario took place on a busy European highway with many scatterers. The analysis includes three different antenna placements. The path loss was modeled for each antenna pair individually. Losses due to the shadowing of the truck were characterized. The large-scale fading distribution and auto-correlation were also described. The RMS delay and Doppler spreads were given as measures of channel dispersion in time and frequency domains respectively. It can be concluded that the dispersion of the channel in both the time and frequency domains increases for the OLOS case.

Another important property to investigate when a truck is blocking vehicular communication is how much power can reach the receiver in the worst case scenario. A model for power contributions solely due to diffraction around the truck has been proposed and validated with real life measurement data. It has been found that there is an area in all from 0 m up to 10 m in-front of the truck were the channel gain is significantly reduced. This area fades out as the vehicle in-front of the truck moves sidewise from the center in-front of the truck and away. This problem can be mitigated by employing antenna diversity, perhaps with one antenna on each side of the car in the door mirrors. By looking at the results it can also be concluded that with diffraction alone it is possible to establish communications at a distance of appr. 300 m, where the channel gain is predicted to be appr. -110 dB. Assuming a transmitter with an effective isotropic radiated power (EIRP) of 20 dBm the received power, not taking antenna gain into consideration, would be -90 dBm, which is above the receiver noise floor for most 802.11p chipsets at the nominal 10 MHz, 6 Mbps rate [69, 70].

A real-time wireless channel emulator based on a software defined radio (SDR) for evaluating the performance of modems for wireless vehicular communications using the 802.11p protocol has been proposed and implemented in chapter 4. Based on the implementation of a tapped-delay line model, a way of performing simple stress tests of modems for vehicular communication

has been presented. Tests with both early prototype modems and dedicated vehicular modems have been performed and their packet error rate (PER) performance has been characterized. Despite expectations, the dedicated modems did not impose a significant improvement over the early prototype modems in the stress tests, only marginal improvements at higher delays were seen. Those improvements might had been larger, if during emulation the second delay tap was attenuated compared to the first delay tap. Both groups of modems performed well at smaller packet sizes. Thus, it may be concluded that safety critical messages should be kept as small as possible, without duplicated information. Unfortunately, that is not currently the case as information such as latitude, longitude, elevation, speed and heading is duplicated in both the CAM [3] and GeoNetworking [4] layers of the Cooperative Awareness Message (CAM) packet.

5.2 Future Work

The road side unit (RSU) presented in chapter 2 is currently only detecting and relaying information for non-wireless enabled vehicles. It can be installed in a plethora of scenarios such as intersections, merging lanes, and more. The implementation can be extended to also relay radio signals from wireless enabled vehicles. In scenarios similar to urban intersection [19], the critical information to prevent a collision would only be received a few seconds prior to a potential collision, due to significant shadowing. By implementing a relay that has LOS with both vehicles in the intersection, the effective range of the system would be greatly increased.

The model for power contributions due to diffraction proposed in chapter 3 is purely theoretical and deterministic. An improvement that could be applied in the future is to consider the current model output as a mean value of the channel gain and provide additionally a stochastic model for the variance of the channel gain assuming some convenient distribution. For this to even be feasible, further measurements with higher dynamic range and higher spatial resolution, both laterally and longitudinally, will have to be performed. Another interesting application of channel models in V2V is their implementation in software that simulates wireless communication in realistic traffic flows, e.g. Veins[1]. By implementing the diffraction model in such simulators, even more realistic simulation results could be obtained. Furthermore, it is interesting to investigate the multilink scenario in V2V communication. Either by simulations using appropriate channel models, or by performing measurements, it is interesting to evaluate whether relaying information from one vehicle to

[1] http://veins.car2x.org/

another is time efficient and beneficial for accident prevention. Nilsson *et al.* in [47, 48] are investigating the multilink scenario.

The SDR–FPGA–based channel emulator described in chapter 4 has already been further improved by Ghiaasi *et al.* in [71]. An array-based implementation of the tapped-delay line model allows for simultaneous activation of more than 2 delay taps, each one having individually controlled amplitude and phase, enabling the implementation of realistic channel models. The design allows for emulation of both stationary and non-stationary channels in vehicular environments. Further development with the addition of a random number generator could allow for the implementation of completely and/or partially stochastic channel models.

References

[1] *IEEE Std. 802.11p-2010, Part 11: Wireless LAN Medium Access Control (MAC) and Physical Layer (PHY) specifications: Amendment 7: Wireless Access in Vehicular Environment*, IEEE Std., July 2010.

[2] "IEEE Standard for Information Technology – Telecommunications and information exchange between systems – Local and metropolitan area networks – Specific requirements – Part 11: Wireless LAN Medium Access Control (MAC) and Physical Layer (PHY) Specifications," *IEEE Std 802.11-2012*, March 2012.

[3] *ETSI TS 102 637-2 Intelligent Transport Systems (ITS); Vehicular Communications; Basic Set of Applications; Part 2: Specification of Cooperative Awareness Basic Service*, European Telecommunications Standards Institute Std., March 2011.

[4] *ETSI TS 102 636-4-1 V1 Intelligent Transport Systems (ITS); Vehicular communications; GeoNetworking; Part 4: Geographical addressing and forwarding for point-to-point and point-to-multipoint communications; Sub-part 1: Media-Independent Functionality*, European Telecommunications Standards Institute Std., Jun 2011.

[5] ETSI-TR-102638, "Intelligent transportation systems (ITS), vehicular communications, basic set of applications, definitions," *V1.1.1*, June 2009.

[6] J. Karedal, F. Tufvesson, N. Czink, A. Paier, C. Dumard, T. Zemen, C. F. Mecklenbrauker, and A. F. Molisch, "A geometry-based stochastic mimo model for vehicle-to-vehicle communications," *IEEE Transactions on Wireless Communications*, vol. 8, no. 7, pp. 3646–3657, July 2009.

[7] Y. Okumura, "Field strength and its variability in uhf and vhf land-mobile radio service," *Review of the Electrical Communication Laboratory*, vol. 16, 1968.

[8] M. Hata, "Empirical formula for propagation loss in land mobile radio services," *IEEE Transactions on Vehicular Technology*, vol. 29, no. 3, pp. 317–325, Aug 1980.

[9] E. Damosso, L. Correia, I. M. European Commission. DGX III "Telecommunications, and E. of Research.", *COST Action 231: Digital Mobile Radio Towards Future Generation Systems: Final Report*, ser. EUR (Series). European Commission, 1999. [Online]. Available: http://www.lx.it.pt/cost231

[10] ITU, "Propagation in non-ionized media," in *Recommendations and Reports of the ITU-R*, Geneva, Switzerland, 2006.

[11] ETSI, "Digital cellular telecommunications system; radio network planning aspects (gsm 03.30 version 5.0.0)," in *ETR 364*, Sophia-Antipolis, France, 1996.

[12] L. M. Correia, "A view of the cost 231-bertoni-ikegami model," in *2009 3rd European Conference on Antennas and Propagation*, March 2009, pp. 1681–1685.

[13] A. F. Molisch, *Wireless Communications*. Wiley, 2011.

[14] R. Failli and COST207, *Digital land mobile radio-communications*, 1989.

[15] ITU, "Guidelines for evaluation of radio transmission technologies for IMT-2000," in *Recommendation ITU-R M.1225*, 1997.

[16] G. Calcev, D. Chizhik, B. Goransson, S. Howard, H. Huang, A. Kogiantis, A. F. Molisch, A. L. Moustakas, D. Reed, and H. Xu, "A wideband spatial channel model for system-wide simulations," *IEEE Transactions on Vehicular Technology*, vol. 56, no. 2, pp. 389–403, March 2007.

[17] ITU, "Guidelines for evaluation of radio interface technologies for IMT-advanced," in *Recommendation ITU-R M.2135*, 2008.

[18] D. Vlastaras, T. Abbas, M. Nilsson, R. Whiton, M. Olbäck, and F. Tufvesson, "Impact of a truck as an obstacle on vehicle-to-vehicle communications in rural and highway scenarios," in *6th International Symposium on Wireless Vehicular Communications*. IEEE, Sep 2014.

[19] T. Abbas, A. Thiel, T. Zemen, C. F. Mecklenbräuker, and F. Tufvesson, "Validation of a non-line-of-sight path-loss model for V2V communications at street intersections," in *13th International Conference on ITS Telecommunications, Tampere, Finland*. IEEE, Nov 2013.

[20] T. Mangel, O. Klemp, and H. Hartenstein, "5.9 GHz inter-vehicle communication at intersections: a validated non-line-of-sight path-loss and fading model," *EURASIP Journal on Wireless Communications and Networking*, vol. 2011, no. 1, p. 182, 2011. [Online]. Available: http://dx.doi.org/10.1186/1687-1499-2011-182

[21] H. El-Sallabi, "Fast path loss prediction by using virtual source technique for urban microcells," in *IEEE 51st Vehicular Technology Conference Proceedings (VTC 2000-Spring)*, vol. 3, Tokyo, Japan, 2000, pp. 2183–2187.

[22] D. Vlastaras, R. Whiton, and F. Tufvesson, "A model for power contributions from diffraction around a truck in vehicle-to-vehicle communications," in *15th International Conference on ITS Telecommunications [Submitted]*, Warsaw, Poland, May 2017.

[23] D. Vlastaras and D. Leston, "Improved traffic safety by wireless vehicular communication," Lund, Sweden, 2013, Master's Thesis.

[24] T. Abbas, "Measurement based channel characterization and modeling for vehicle-to-vehicle communications," Ph.D. dissertation, Department of Electrical and Information Technology, Faculty of Engineering, Lund University, 2014.

[25] M. S. Short, G. A. Woelfl, and C.-J. Chang, "Effects of traffic signal installation on accidents," *Accident Analysis & Prevention*, vol. 14, no. 2, pp. 135–145, 1982. [Online]. Available: http://www.sciencedirect.com/science/article/pii/000145758290080X

[26] N. Stamatiadis, W. C. Taylor, and F. X. McKelvey, "Elderly drivers and intersection accidents," *Transportation Quarterly*, vol. 45, no. 3, p. 377, Jul 1991.

[27] M. Poch and F. Mannering, "Negative binomial analysis of intersection-accident frequencies," *Journal of Transportation Engineering*, vol. 122, no. 2, pp. 105–113, 1996.

[28] E. Belyaev, P. Molchanov, A. Vinel, and Y. Koucheryavy, "The use of automotive radars in video-based overtaking assistance applications," *IEEE Transactions on Intelligent Transportation Systems*, vol. 14, no. 3, pp. 1035–1042, 2013.

[29] *UMRR Traffic Management Sensor Full Documentation*, Smart Microwave Sensors GmbH, Germany, 2012.

[30] *CAN Specification*, Robert Bosch GmbH, Germany, 1991.

[31] *ETSI TS 102 636-4-1 V1.1.1*, European Telecommunications Standards Institute, France, 2011.

[32] *ETSI TS 102 636-5-1 V1.1.1*, European Telecommunications Standards Institute, France, 2011.

[33] *Topcon GRS-1, GNSS Receiver and Field Controller, Brochure*, Topcon Positioning Systems, Inc., USA, 2013.

[34] D. W. Allan, N. Ashby, and C. C. Hodge, "The science of timekeeping, application note 1289," 1997.

[35] D. Mills, U. Delaware, J. M. Ed, ISC, J. Burbank, W. Kasch, and JHU/APL, "Network time protocol version 4: Protocol and algorithms specification (rfc5905)," 2010.

[36] *Leap Seconds*, Time Service Department, U.S. Naval Observatory, Washington, DC, USA, 2012.

[37] D. Gambis, "Bulletin C 43," *Earth Orientation Center of International Earth Rotation and Reference Systems Service (IERS)*, 2012.

[38] R. E. Kalman, "A new approach to linear filtering and prediction problems," *Transactions of the ASME–Journal of Basic Engineering*, vol. 82, no. Series D, pp. 35–45, 1960.

[39] F. Gustafsson, *Statistical Sensor Fusion*. Lund, Sweden: Studentlitteratur, 2010.

[40] G. Welch and G. Bishop, "An introduction to the Kalman filter," Department of Computer Science, University of North Carolina at Chapel Hill, Tech. Rep., 2006.

[41] A. Paier, L. Bernado, J. Karedal, O. Klemp, and A. Kwoczek, "Overview of vehicle-to-vehicle radio channel measurements for collision avoidance applications," in *Vehicular Technology Conference (VTC 2010-Spring), IEEE 71st, Taipei, Taiwan*, May 2010, pp. 1–5.

[42] R. Meireles, M. Boban, P. Steenkiste, O. Tonguz, and J. Barros, "Experimental study on the impact of vehicular obstructions in VANETs," in *IEEE Vehicular Networking Conference (VNC), New Jersey, USA*, Dec 2010, pp. 338–345.

[43] M. Boban, T. Vinhoza, M. Ferreira, J. Barros, and O. Tonguz, "Impact of vehicles as obstacles in vehicular ad hoc networks," *IEEE Journal on Selected Areas in Communications*, vol. 29, no. 1, pp. 15–28, Jan 2011.

[44] T. Abbas, K. Sjöberg, J. Karedal, and F. Tufvesson, "A measurement based shadow fading model for vehicle-to-vehicle network simulations," *International Journal of Antennas and Propagation*, vol. 2015, 2015.

[45] M. Segata, B. Bloessl, S. Joerer, C. Sommer, R. L. Cigno, and F. Dressler, "Vehicle shadowing distribution depends on vehicle type: Results of an experimental study," in *5th IEEE Vehicular Networking Conference (VNC 2013)*. Boston, MA: IEEE, December 2013, pp. 242–245.

[46] R. He, A. F. Molisch, F. Tufvesson, Z. Zhong, B. Ai, and T. Zhang, "Vehicle-to-vehicle propagation models with large vehicle obstructions," *IEEE Journal on Intelligent Transportation Systems*, vol. 15, no. 5, pp. 2237–2248, 2014.

[47] M. G. Nilsson, D. Vlastaras, T. Abbas, B. Bergqvist, and F. Tufvesson, "On multilink shadowing effects in measured V2V channels on highway," in *9th European Conference on Antennas and Propagation (EuCAP)*, May 2015, pp. 1–5.

[48] M. G. Nilsson, C. Gustafson, T. Abbas, and F. Tufvesson, "A measurement based multilink shadowing model for V2V network simulations of highway scenarios [in review]," *IEEE Transactions on Vehicular Technology*, 2017.

[49] A. F. Molisch, F. Tufvesson, J. Karedal, and C. F. Mecklenbräuker, "A survey on vehicle-to-vehicle propagation channels," *Wireless Communications, IEEE*, vol. 16, no. 6, pp. 12–22, 2009.

[50] T. Abbas, F. Tufvesson, and J. Karedal, "Measurement based shadow fading model for vehicle-to-vehicle network simulations," *ArXiv e-prints*, Mar 2012.

[51] B. Gallagher, H. Akatsuka, and H. Suzuki, "Wireless communications for vehicle safety: Radio link performance and wireless connectivity methods," *Vehicular Technology Magazine, IEEE*, vol. 1, no. 4, pp. 4–24, 2006.

[52] K. Mahler, W. Keusgen, F. Tufvesson, T. Zemen, and G. Caire, "Propagation channel in a rural overtaking scenario with large obstructing vehicles," in *IEEE 83rd Vehicular Technology Conference*, May 2016, pp. 1–5.

[53] R. Thoma, D. Hampicke, A. Richter, G. Sommerkorn, A. Schneider, U. Trautwein, and W. Wirnitzer, "Identification of time-variant directional mobile radio channels," *Instrumentation and Measurement, IEEE Transactions on*, vol. 49, no. 2, pp. 357–364, Apr 2000.

[54] T. Abbas, J. Karedal, and F. Tufvesson, "Measurement-based analysis: The effect of complementary antennas and diversity on vehicle-to-vehicle communication," *IEEE Antennas and Wireless Propagation Letters*, vol. 12, no. 1, pp. 309–312, 2013.

[55] J. Karedal, N. Czink, A. Paier, F. Tufvesson, and A. Molisch, "Path loss modeling for vehicle-to-vehicle communications," *IEEE Transactions on Vehicular Technology*, vol. 60, no. 1, pp. 323–328, 2011.

[56] T. Abbas, C. Gustafson, and F. Tufvesson, "Pathloss estimation techniques for incomplete channel measurement data," in *COST IC1004 10th Management Committee and Scientific Meeting*, 2014. [Online]. Available: http://lup.lub.lu.se/record/4442929/file/4461934.pdf

[57] A. P. Dempster, N. M. Laird, and D. B. Rubin, "Maximum likelihood from incomplete data via the EM algorithm," *Journal of the Royal Statistical Society, Series B*, vol. 39, no. 1, pp. 1–38, 1977.

[58] M. Gudmundson, "Correlation model for shadow fading in mobile radio systems," *Electronics Letters*, vol. 27, no. 23, pp. 2145–2146, Nov 1991.

[59] A. Goldsmith, *Wireless Communications*. Cambridge: Cambridge University Press, 8 2005. [Online]. Available: https://www.cambridge.org/core/books/wireless-communications/800BA8A8211FBECB133A7BB77CD2E2BD

[60] E. J. Jaselskis, J. Grigas, and A. Brilingas, "Dielectric properties of asphalt pavement," *Journal of Materials in Civil Engineering*, vol. 15, no. 5, pp. 427–434, 2003. [Online]. Available: http://dx.doi.org/10.1061/(ASCE)0899-1561(2003)15:5(427)

[61] J. Epstein and D. W. Peterson, "An experimental study of wave propagation at 850 MC," *Proceedings of the IRE*, vol. 41, no. 5, pp. 595–611, May 1953.

[62] *Device Specifications, NI USRP-2943R, 1.2 GHz to 6 GHz Tunable RF Transceiver*, National Instruments.

[63] (2013, May) Real-time MIMO channel emulation on the NI PXIe-5644R. National Instruments. Accessed 2017-01-22. [Online]. Available: http://www.ni.com/example/31556/en/

[64] M. Nilsson, P. Hallbjörner, N. Arabäck, B. Bergqvist, and F. Tufvesson, "Multipath propagation simulator for V2X communication tests on cars,"

in *Antennas and Propagation (EuCAP), 2013 7th European Conference on*. IEEE, Apr 2013, pp. 1342–1346.

[65] M. Gurcan, "Rapid prototyping for 5G transmission system emulation," in *IEEE Global Communications Conference*. Austin, USA: IEEE, Dec 2014, industry program demonstration.

[66] Accessed 2017-01-22. [Online]. Available: http://www.spirent.com/

[67] Accessed 2017-01-22. [Online]. Available: http://www.anite.com/

[68] *IEEE Standard for Information technology - Telecommunications and information exchange between systems, Local and metropolitan area networks - Specific requirements. Part 11: Wireless LAN Medium Access Control (MAC) and Physical Layer (PHY) Specifications*, IEEE Std., Rev. IEEE Std 802.11-2012, March 2012.

[69] *Product Specification, Test Modem*, Kapsch TrafficCom AB, Sweden, 2012.

[70] Kapsch, EVK-3300, V2X Evaluation Kit. Accessed 2017-01-22. [Online]. Available: http://www.kapsch.net/ktc/downloads/datasheets/v2x/Kapsch-KTC-DS-EVK-3300-EN-WEB?lang=en-US

[71] G. Ghiaasi, M. Ashury, D. Vlastaras, M. Hofer, Z. Xu, and T. Zemen, "Real-time vehicular channel emulator for future conformance tests of wireless its modems," in *10th European Conference on Antennas and Propagation (EuCAP)*, April 2016, pp. 1–5.